UNITED NATIONS EDUCATIONAL, SCIENTIFIC AND CULTURAL ORGANIZATION
INTERNATIONAL ATOMIC ENERGY AGENCY
INTERNATIONAL CENTRE FOR THEORETICAL PHYSICS
I.C.T.P., P.O. BOX 586, 34100 TRIESTE, ITALY, CABLE: CENTRATOM TRIESTE

H4.SMR/916 - 24

SEVENTH COLLEGE ON BIOPHYSICS:
Structure and Function of Biopolymers: Experimental and Theoretical Techniques.
4 - 29 March 1996

Nucleic Acids: Structural Aspects

Franco QUADRIFOGLIO
Dept. Biomedical Sciences and Technologies
School of Medicine
University of Udine
Udine

Franco Quadrifoglio
Dept. Biomedical Sciences and Technologies
School of Medicine
University of Udine

Nucleic Acids: Structural Aspects
(Lecture Notes)

MAIN BUILDING STRADA COSTIERA, 11 TEL. 224011 TELEFAX 224163 TELEX 460392 ADRIATICO GUEST HOUSE VIA GRIGNANO, 9 TEL. 224241 TELEFAX 224531 TELEX 460449
MICROPROCESSOR LAB VIA BEIRUT, 31 TEL. 224911 TELEFAX 224600 TELEX 460392 GALILEO GUEST HOUSE VIA BEIRUT, 7 TEL. 224011 TELEFAX 224010 TELEX 460392

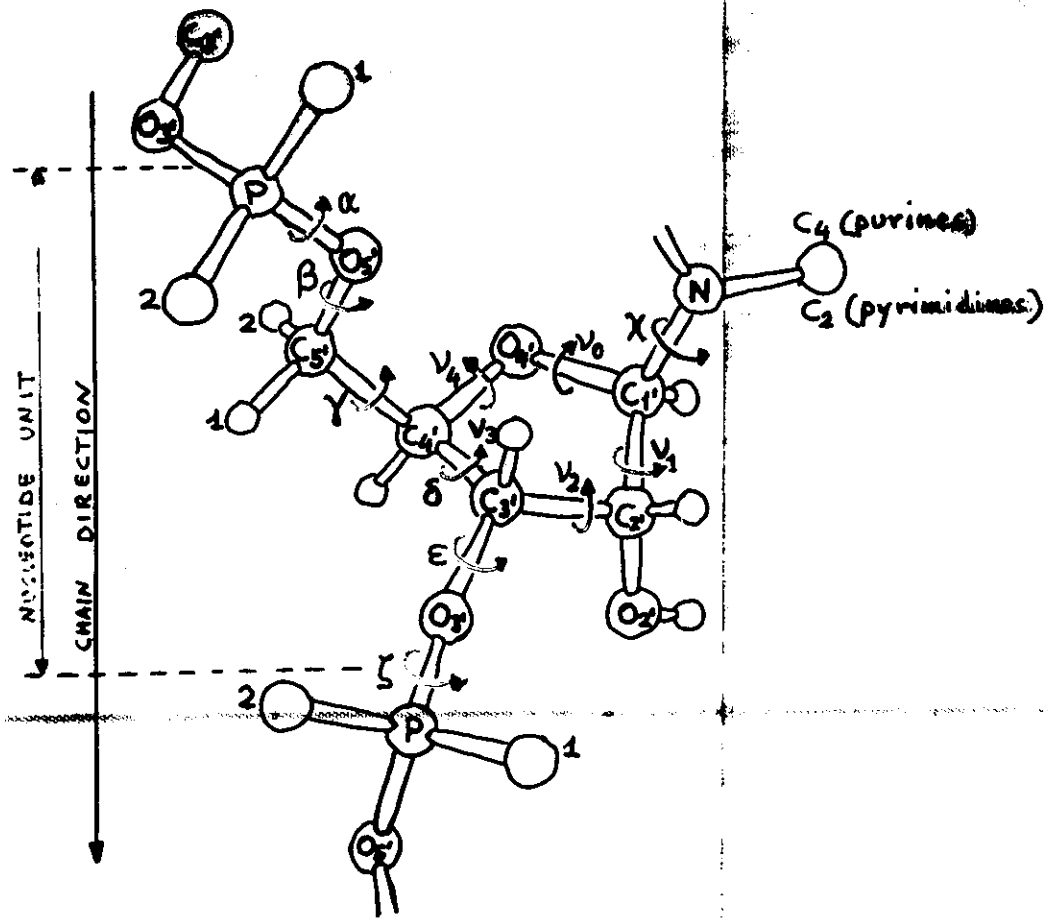

IF (A) IS ECLIPSED WITH (D) $\theta = 0$

θ IS POSITIVE WHEN THE FAR BOND IS ROTATED CLOCKWISE

TABLE I

DEFINITION OF TORSION ANGLES IN NUCLEOT.

TORSION ANGLES	ATOMS INVOLVED
α	$O_{3'} - P - O_{5'} - C_{5'}$
β	$P - O_{5'} - C_{5'} - C_{4'}$
γ	$O_{5'} - C_{5'} - C_{4'} - C_{3'}$
δ	$C_{5'} - C_{4'} - C_{3'} - O_{3'}$
ε	$C_{4'} - C_{3'} - O_{3'} - P$
ζ	$C_{3'} - O_{3'} - P - O_{5'}$
χ	$O_{4'} - C_{1'} - N_1 - C_2$ (PYR) $O_{4'} - C_{1'} - N_9 - C_4$ (PUR)
ν_0	$C_{4'} - O_{4'} - C_{1'} - C_{2'}$
ν_1	$O_{4'} - C_{1'} - C_{2'} - C_{3'}$
ν_2	$C_{1'} - C_{2'} - C_{3'} - C_{4'}$
ν_3	$C_{2'} - C_{3'} - C_{4'} - O_{4'}$
ν_4	$C_{3'} - C_{4'} - O_{4'} - C_{1'}$

SUGAR PUCKERING

^3E $C_{3'}$ ENDO CALLED ALSO N

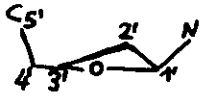

^2E $C_{2'}$ ENDO CALLED ALSO S

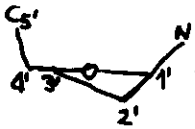

$_2E$ $C_{2'}$ EXO

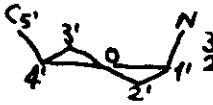

^3_2T $C_{2'}$ EXO-$C_{3'}$ ENDO

$C_{3'}$ ENDO AND $C_{2'}$ ENDO ARE, BY FAR, THE MOST PREFERRED CONFORMATIONS.
THIS IS DUE TO THE LOWER ROTATION BARRIERS AROUND C-O BONDS WITH RESPECT TO C-C BONDS
THEREFORE ν_0 AND ν_4 ARE NEARLY ECLIPSED, WHEREAS ν_1, ν_2 AND ν_3 ARE MAXIMALLY STAGGERED.

Fig. 2.1

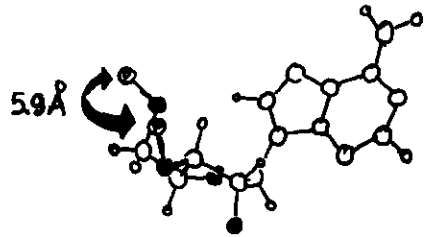

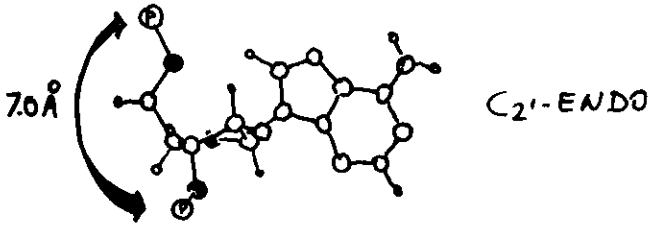

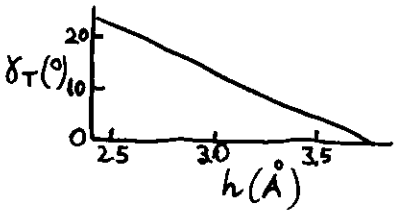

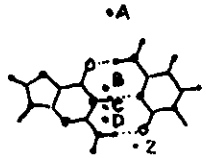

FIG. 2.2

SYN-ANTI ORIENTATION OF THE N-GLYCOSIDIC BOND

PURINE

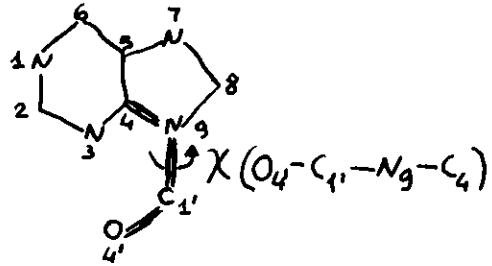

$\chi \simeq 0°$ SYN

PYRIMIDINE

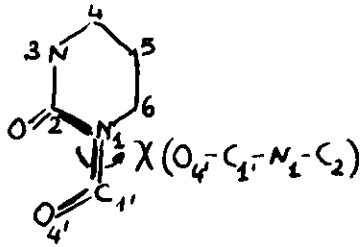

$\chi \simeq 180°$ ANTI!

ANTI

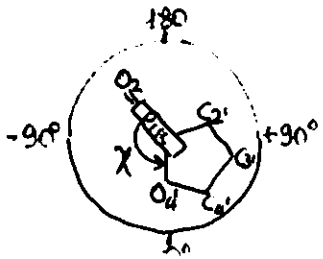

SYN

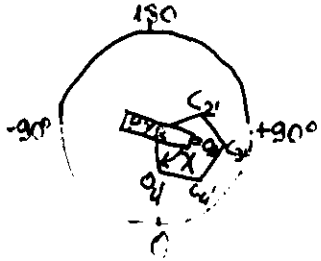

- PURINE NUCLEOTIDES CAN ADOPT BOTH SYN AND ANTI CONFORMATIONS WHEN SUGAR PUCKERING IS C2'ENDO
- PURINE NUCLEOTIDES PREFER ANTI WHEN SUGAR IS C3'ENDO
- PYRIMIDINES NUCLEOTIDES ARE MOSTLY ANTI WHEN RIBOSE IS C3'ENDO OR DEOXYRIBOSE IS C2'ENDO

Fig. 3

TORSION ANGLE AROUND $C_{4'}-C_{5'}$ BOND

ROTATION AROUND THIS BOND DEFINES THE POSITION OF THE PHOSPHATE GROUP WITH RESPECT TO BASE AND SUGAR

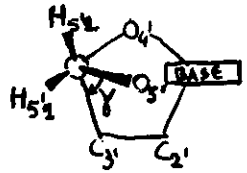

+ SC (THE MOST PREFERRED)

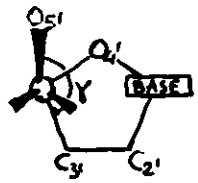

ap

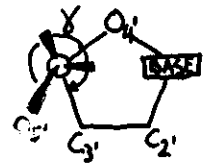

-SC

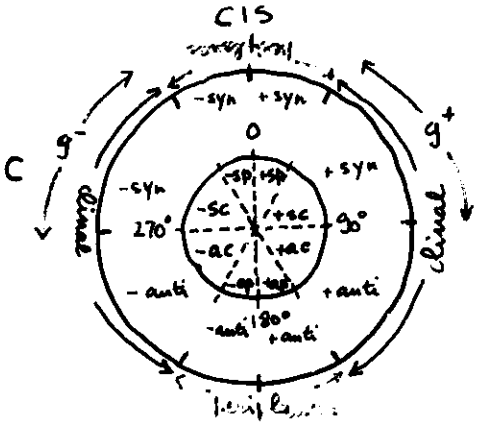

a = anti
s = syn
p = periplanar
c = clinal

Fig. 4

TORSION ANGLES AROUND C-O BONDS IN POLYNUCLEOT.

$C_{5'}-O_{5'}$ β IS ESSENTIALLY ap (trans, 180°)

$C_{3'}-O_{3'}$ ε IS ap (trans, 180°) OR -ac (~220°)

TORSION ANGLES AROUND P-O BONDS IN POLYNUCLEOT.

$P-O_{5'}$ α IS -sc (gauche⁻, -50°/-90°)

$P-O_{3'}$ ζ IS -sc (gauche⁻, -50°/-90°)

IN HELICAL POLYNUCLEOTIDES ALL BACKBONE TORSIONAL ANGLES ARE CORRELATED.

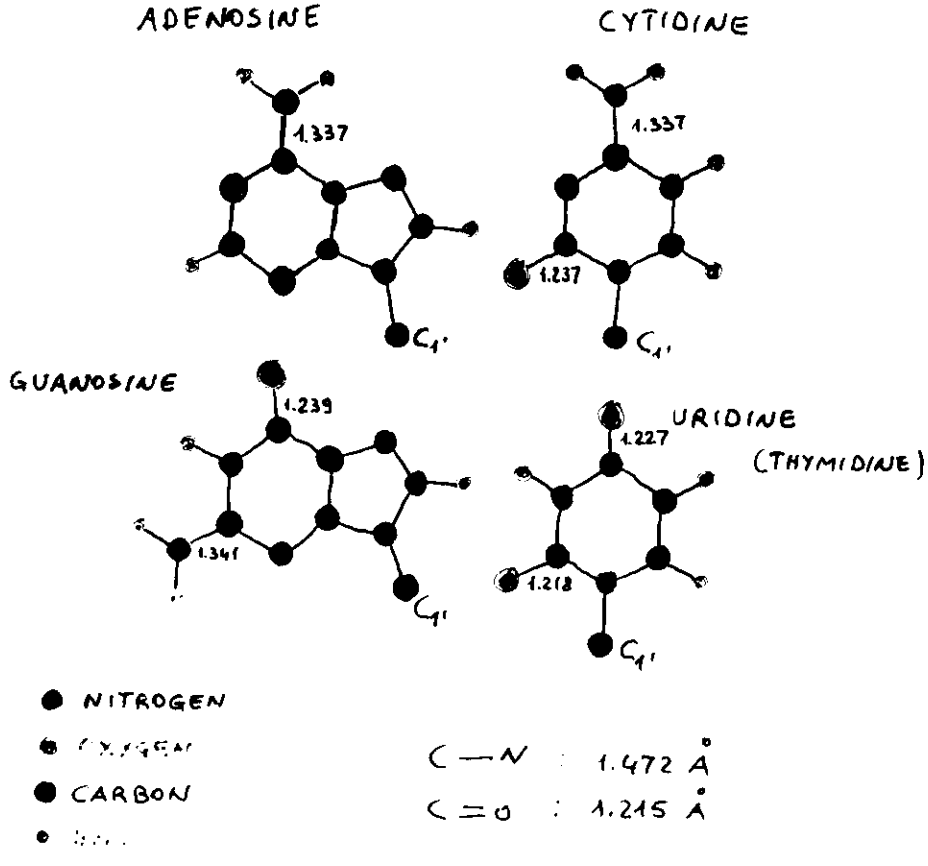

Fig. 5

FIG. 5.1

PROTONATION AND DEPROTONATION OF BASES OCCUR WITHIN 3.2 pH UNITS FROM NEUTRALITY, THAT IS BETWEEN 3.5 AND 10.5. THIS INDICATES THAT AMIDE-LIKE HYDROGENS (N_3 OF URACIL AND N_1 OF GUANINE) ARE RATHER ACIDIC IN CHARACTER AND RING NITROGENS ARE BASIC.

IN NUCLEOTIDES, DUE TO THE ELECTROSTATIC ATTRACTION OF THE NEGATIVELY CHARGED PHOSPHATES AT DIFFERENT DISTANCES FROM THE BASES, THE pK VALUES OF THE BASES INCREASE BY ABOUT 0.5 UNIT WHEN GOING FROM NUCLEOSIDE TO 3'-NUCLEOTIDE OR TO 5' NUCLEOTIDE

	NUCLEOSIDE	3'-PHOSPHATE	5'-P
ADENOSINE / N_1	3.52	3.70	3.85
CYTIDINE / N_3	4.17	4.43	4.56
GUANOSINE / N_1	9.42	9.84	10.00
URIDINE / N_3	9.38	9.96	10.06
2'-DEOXYTHYMIDINE / N_3	9.93	-	10.47

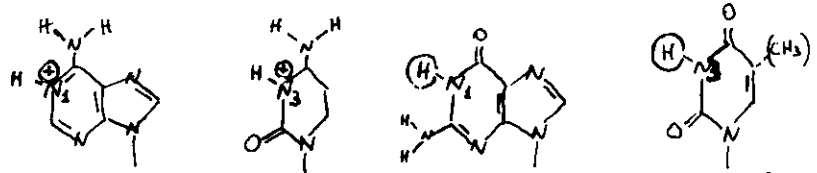

[pH LOWER THAN 2 N_7 OF GUANINE AND ADENINE AS WELL AS O_4 OF URACIL (THYMINE) ARE PROTONATED-

RIBONUCLEOTIDES (NOT DEOXY-) ARE DEPROTONATED AT 2'-3' HYDROXYL AT pH > 12.5.

FIG. 5.2

TAUTOMERISM OF BASES

KETO ⇌ ENOL TAUTOMERISM

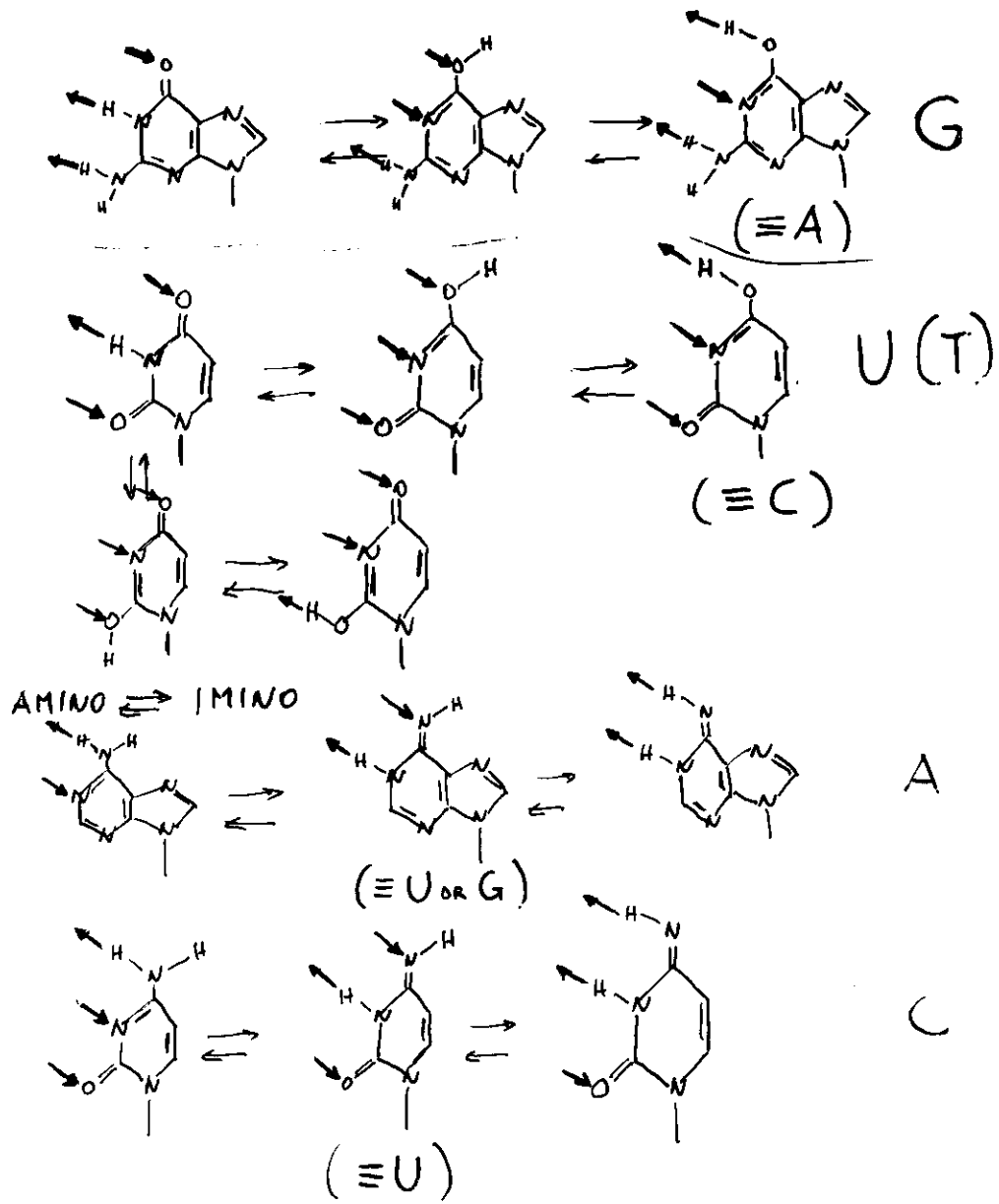

ENOL AND IMINO FORMS EXIST IN LESS THAN 0.01% RANGE

FIG. 5.3

HYDROGEN BONDS

X—H ---- Y

PREVALENTLY ELECTROSTATIC IN CHARACTER

N—H ··· N
N—H ··· O
} IN NATURALLY OCCURRING BASES

SOMETIMES BIFURCATED HYDROGEN BONDS CAN OCCUR

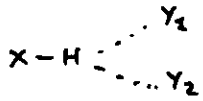

UNDER THE INFLUENCE OF A HYDROGEN BOND, THE CHARGES ON THE ATOMS INVOLVED ARE MODIFIED DUE TO POLARIZATION. H BECOMES MORE POSITIVE AND X, Y MORE NEGATIVE THEREFORE X AND Y HAVE INCREASED AFFINITY TO ACCEPT FURTHER HYDROGEN BONDS. IN CYCLIC STRUCTURES A COOPERATIVE EFFECT IS OCCURRING:

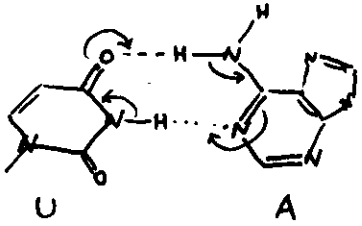

U A

UNDER THE ASSUMPTION THAT AT LEAST TWO CYCLIC HYDROGEN BONDS MUST FORM IN ORDER TO PRODUCE A STABLE PAIR, THE FOUR ~~BASE~~ NUCLEOSIDES CAN BE ARRANGED IN 28 DIFFERENT WAYS.

FIG. 6

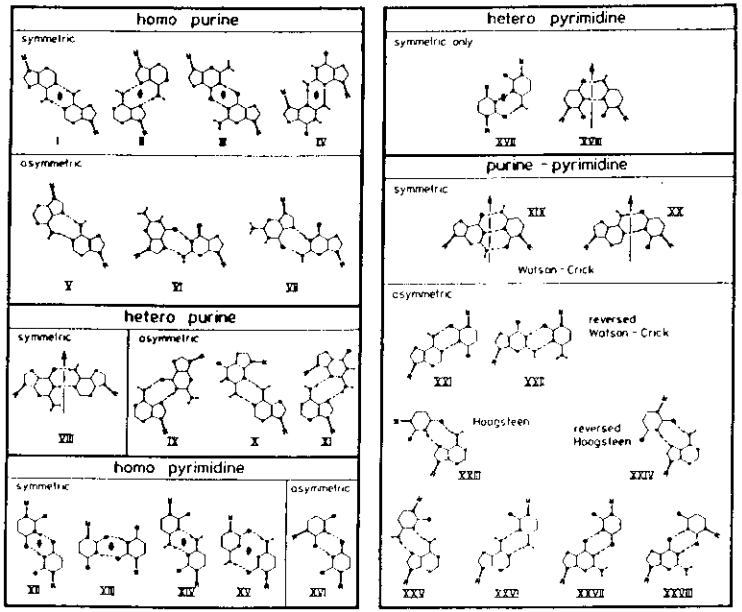

FIG. 6.1

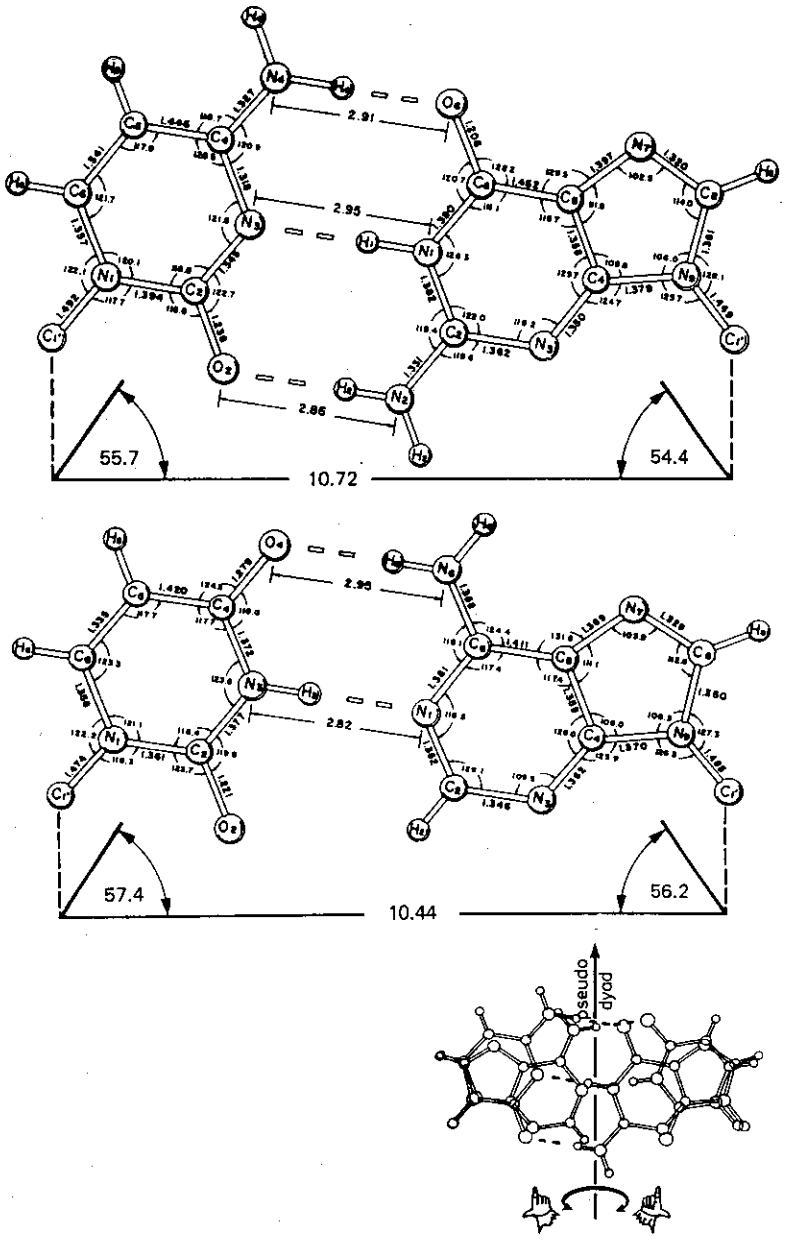

Fig. 6.2

DOUBLE-HELICAL POLYNUCLEOTIDES ARE FORMED BY TWO ANTIPARALLEL STRANDS JOINED BY HYDROGEN BONDS BETWEEN COMPLEMENTARY BASES

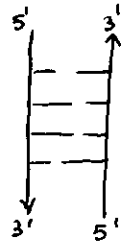

IF THE TORSION ANGLES AROUND THE SINGLE BONDS PRESENT A REGULARITY ALONG THE POLYNUCLEOTIDE BACKBONE THE RESULTING STRUCTURE RESULTS ORDERED AND HELICAL.

THE STRUCTURE CAN BE DERIVED FROM X-RAY DIFFRACTION OF FIBERS PULLED FROM CONCENTRATED SOLUTION UNDER DEFINITE CONDITIONS OF IONIC STRENGTH, TYPE OF COUNTERION AND RELATIVE HUMIDITY.

TYPE OF NUCLEOTIDE CHAINS (DNA OR RNA) AND BASE SEQUENCE INFLUENCE ALSO THE FINAL STRUCTURE.

FIG. 7

Table 9-1. Principal Crystalline Forms of DNA and RNA in Fibers: Dependence of Form and Helix Symmetry on Counterion and Relative Humidity (Equivalent to Salt Concentration)[a]

Polynucleotide	Counterion	Relative humidity (%)	Form	Helix symmetry	Reference
Native DNA	Na	75	A	11_1	(842)
	Na	92	B	10_1	(101)
	Li	57–66	C	$9.33_1(28_3)$	(94)
	Li	44	C	$9.33_1(28_3)$	(94)
	Li	66	B	10_1	(824)
Poly(dA)·poly(dT)	Na	70	β–B′	10_1	(843)
	Na	92	α–B′	10_1	(843)
Poly(dG)·poly(dC)	Na	75	A	11_1	(844)
	Na	92	B	10_1	(844)
Poly(dA–dT)·poly(dA–dT)	Na	75	D	8_1	(845)
	Na	Up to 98	A	11_1	(846)
	Li	66	B	10_1	(846)
Poly(dA–dC)·poly(dG–dT)	Na	66	A	11_1	(824)
	Na	66–92	B	10_1	(824)
	Na	66	Z	6_5	(304)
Poly(dA–dG)·poly(dC–dT)	Na	66	C″	9_1	(824)
	Na	95	B	10_1	(824)
Poly(dG–dC)·poly(dG–dC)	Na	43	Z	6_5	(304)
	Na	Up to 92	A	11_1	(824)
	Li	81	B	10_1	(824)
Poly(dA–dA–dT)·poly(dA–dT–dT)	Na	66	D	8_1	(847)
	Na	92	B	10_1	(847)
Poly(dA–dG–dT)·poly(dA–dC–dT)	Na	Up to 98	A	11_1	(824)
	Li	98	B	10_1	(824)
	Li	66	C	9_1	(824)
Poly(dA–dI–dT)·poly(dA–dC–dT)	Na	66	D	8_1	(824)
	Na	81	C	$9.33_1(28_3)$	(824)
	Na	92	B	10_1	(824)
Poly(dI–dC)·poly(dI–dC)	Na	66	B	10_1	(388)
	Na	75	D	8_1	(388)
Native RNA (reovirus)	Na	Up to 92	A	11_1	(848)
Poly(A)·poly(U)	Na	Up to 92	A	11_1	(848)
Poly(I)·poly(C)	Na	Up to 92	A′	12_1	(848)
Hybrid poly(rI)·poly(dC)[b]	Na	75	A′	12_1	(849)
Hybrid DNA–RNA	Na	33–92	A	11_1	(850)
Phage T2 DNA	Na	60	T	8_1	(858)

[a] In the original literature (824), more data are entered, and in (304) the notation S-DNA instead of Z-DNA is used.
[b] Helical parameters not mentioned in (849) but in (851).

FIG. 7.1

Polynucleotide	Helix type	Helix symmetry[a]	Pitch height (Å)	Axial rise per residue (Å)	Rotation per residue (°)	Dislocation[b] *D* (Å)	Tilt (°)	Reference
Heteropolymer double helices								
α-A-RNA } reovirus	A	11_1	30.0	2.73	32.7	4.4	17.0 }	(852)
β-A-RNA } reovirus	A	11_1	30.0	2.73	32.7	4.4	19.2 }	
Poly(A)·poly(U)	A	11_1	30.9	2.81	32.7	4.4	16.0 }	(848)
Poly(I)·poly(C)	A′	12_1	36.0	3.00	30.0	4.4	10.0 }	
A-DNA	A	11_1	28.2	2.56	32.7	4.7	20.0	(843)
Poly(2-methylthio-A)·poly(U) with Hoogsteen base-pairs } Poly(ms^2A)	A							
Poly(U)	A	10_1	31.6	3.16	36.0	—	13	(887)
							10	
Heteropolymer triple helices								
Poly(dT)·poly(dA)·poly(dT) Watson–Crick, Hoogsteen	A′	12_1	39.1	3.26	30.0	2.80 Watson–Crick	8.5	
Poly(U)·poly(A)·poly(U)								
92% relative humidity	A′	12_1	36.5	3.04	30.0			(853)
72% relative humidity	A	11_1	33.4	3.04	32.7		12.0	
Poly(I)·poly(A)·poly(I)	A	11_1	36.2	3.29	32.7	2.8	12.0 8.0	
DNA–RNA hybrids								
Poly(rI)·poly(dC)	A′	12_1	35.6	2.97	— 30	4.9	5.68	(849)
Poly(U)·poly(dA)·poly(U)	A	11_1	33.6	3.06	32.7		12.0	(853)
Poly(dC)·poly(I)·poly(dC)	A	11_1	34.8	3.16	32.7		10.0	
Homopolymer complexes								
Poly(AH^+)·poly(AH^+)	A	8_1	30.4	3.8	45		10	(458)
Poly(s^2U)·poly(s^2U)	A	11_1	28.8	2.62	32.7		18	(461)
Poly(X)·poly(X)								
pH 5.7	A	10_1	30.1	3.01	36		21	(854)
pH 8.0		11_1	27.7	2.52	32.7		11	
$[Poly(I)]_4 \cdot [poly(G)]_4$	A	23_2	39.2	3.41	31.3		11	(855)
Homopolymer single helices								
Poly(C)	A	6_1	18.6	3.1	60	—	21	(947)
Poly(O_2-methyl-C)	A	6_1	18.9	3.2	60	—	28	
Poly(A)								
Twofold	—	2_1	5.8	2.9	180	—	36	(963)
Ninefold	A	9_1	25.4	2.82	40	—	24	(957)
B-DNA	B	10_1	33.7	3.37	36	−0.14	−5.9/−2.1	(843,856)
C-DNA	C	28_3	30.9	3.31	38.6	−1.0	−8.0/1.0	(842,857)
Poly(dA-dT)·poly(dA-dT)	D	8_1	24.2	3.03	45	−1.8	−16.4	(845)
T2-DNA	D	8_1	27.2	3.40	45	−1.43	−6/4	(858)
Poly(dA)·poly(dT)	B′	10_1	32.9	3.29	36	−0.02	−7.9/−1.0	(859)
"Alternating" B-DNA								
Homopolymer single helix								
Poly(dT)	—	7.2_1	25.2	3.5	50		132	(358)
DNA·RNA hybrid at high relative humidity								
Poly(A)·poly(dT)								
Poly(A) (C_3-*endo* sugar pucker)	B	9.7_1	33.7	3.46	37.0	—	—	(912)
Poly(DT)	B							

[a] For explanation, see Box 9-1.
[b] Defined in Figure 2-14.
[c] Gives the angle between normal to plane of base and helix axis. If two numbers separated by a slash are given, the first denotes base-pair tilt θ_T, the second propeller twist θ_P of bases relative to each other (see Figure 2-14).
[d] Original assignment as C_3-*endo*-type sugar (993) later proved erroneous (855).

FIG. 7.2

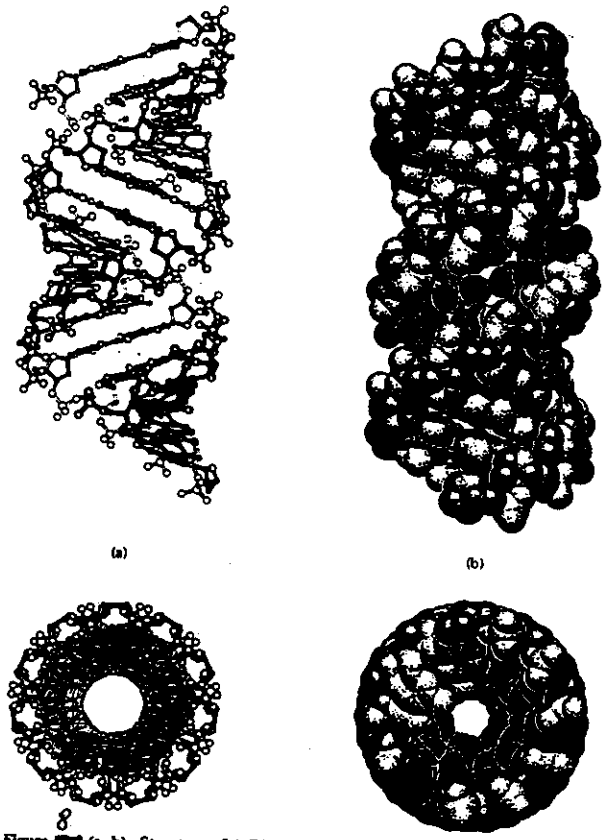

8

Figure 8-1 (a, b). Structure of A-DNA drawn with coordinates from (843). Computer plots are side and top views of A-DNA in (a) ball and stick, and (b) space filling representations. If the helix is tilted about 30° from the viewer to give an impression of the shapes of minor and major grooves, a picture similar to Figure 10-1 (right) is obtained. For graphical details and scale, see the legend to Figure 10-1. In the space filling plot (b), the same input as for the ball-and-stick drawing is used; atomic radii are C = 1.6 Å, N = 1.5 Å, and O = 1.4 Å. Hydrogen atoms are omitted. A light source shines on the molecule under an angle of 45° from the top. Note that the deep, narrow major groove appears dark because it is in shadow.

Fig. 8.1

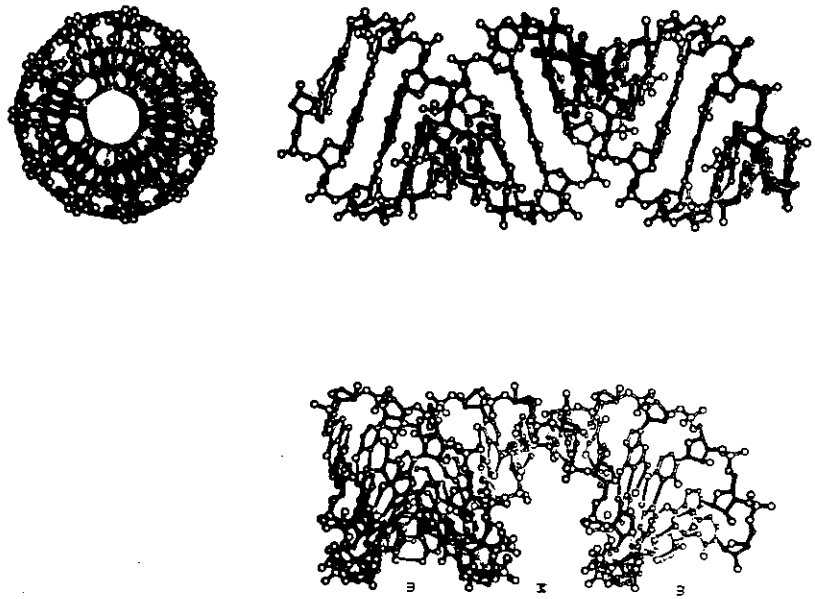

Figure 10-1. Illustration of the molecular structure of A-RNA, drawn with computer program SCHAKAL (1376) according to coordinates given in (848). Circles of increasing radius indicate C,N,O atoms; hydrogens are omitted for clarity. The ribose–phosphate backbone is drawn in black, the bases in color, and the base-pair hydrogen bonds in gray. Scale: 1 cm = 5 Å. Parts closer to the viewer are indicated in heavier lines. (left) Views are perpendicular and parallel to the helix axis. (right) The double helix is tilted by 32° to show the depth of the major groove (M) and the shallowness of the minor groove (m).

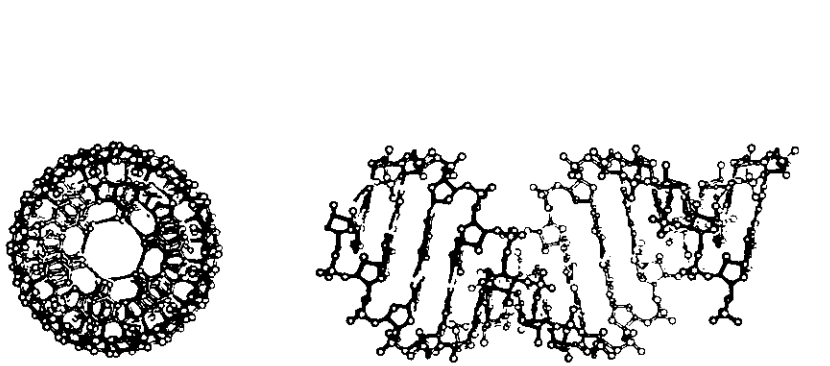

Figure 10-2. The structure of A-RNA, drawn with atomic coordinates published in (848). For further details, see the legend to Figure 10-1.

FIG. 8.2

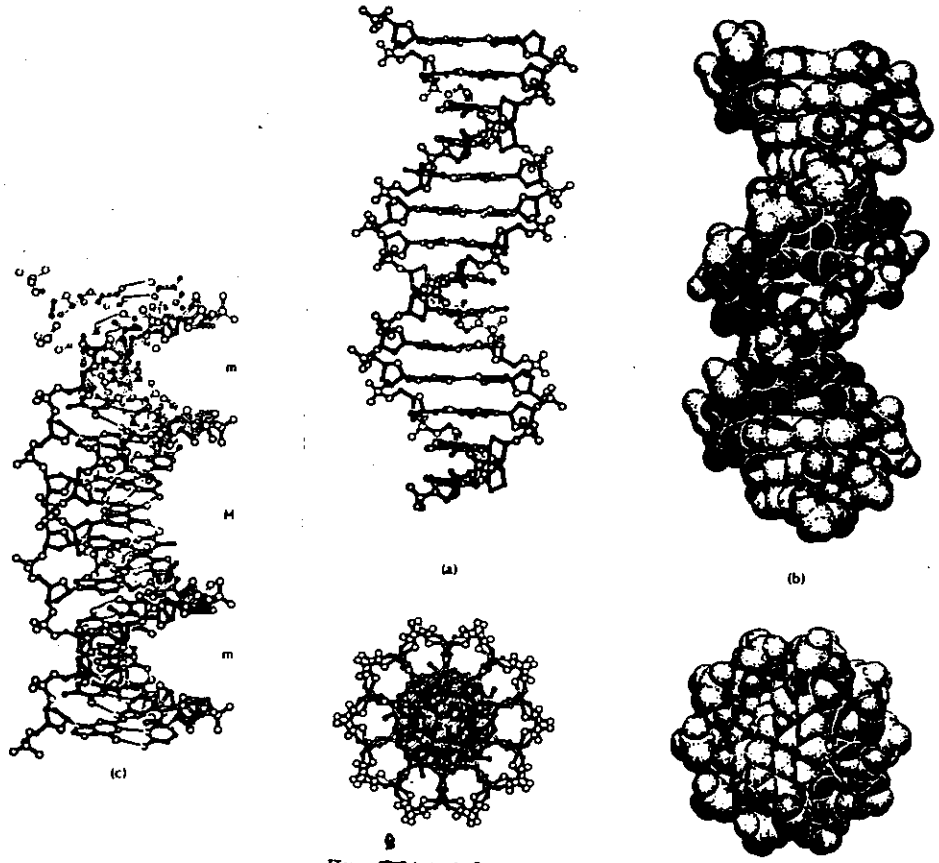

Figure [illegible] (a to c). Structure of B-DNA drawn with coordinates supplied by Drs. S. Arnott and R. Chandrasekaran (1981). For graphical details and scale, see legend to Figure 11-2. (a and b) Side and top view of B-DNA in ball-and-stick and space filling representation; (c) the helix tilted 32° from the viewer to show minor (m) and major (M) grooves.

Fig. 9

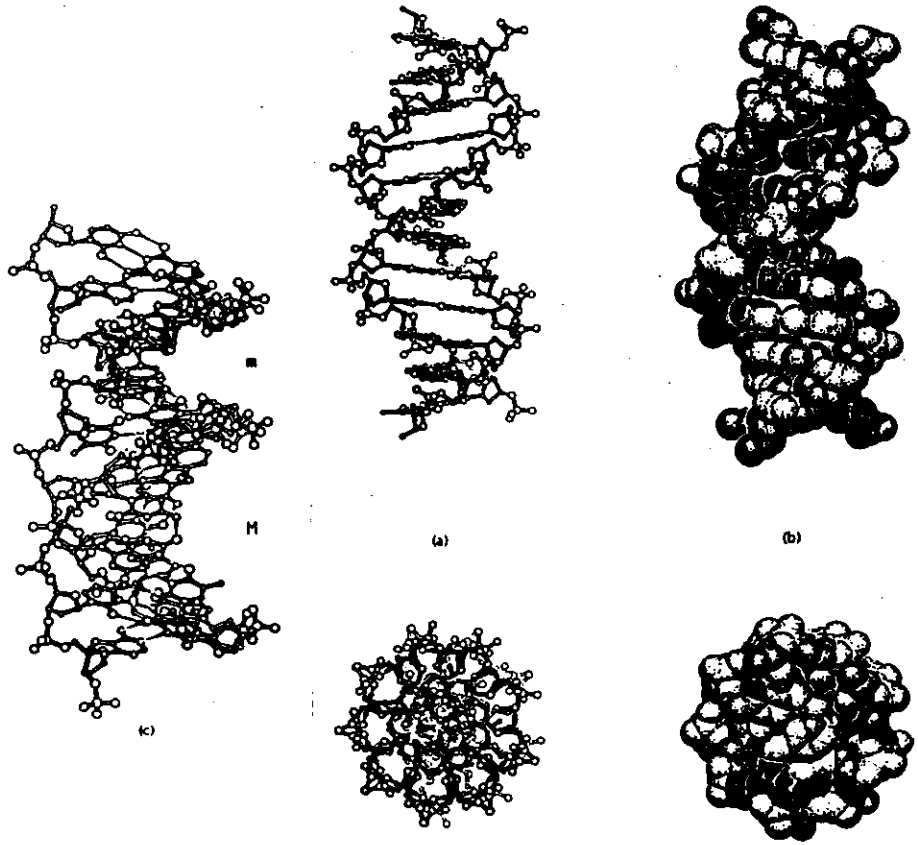

10

Figure [illegible] (a to c). Structure of C-DNA drawn with atomic coordinates given in (94). For graphical details and scale, see the legend to Figure 11-2. (a and b) Side and top view of C-DNA in ball-and-stick and space filling representation. (c) The helix tilted 32° from the viewer to show minor (m) and major (M) grooves.

Fig. 10

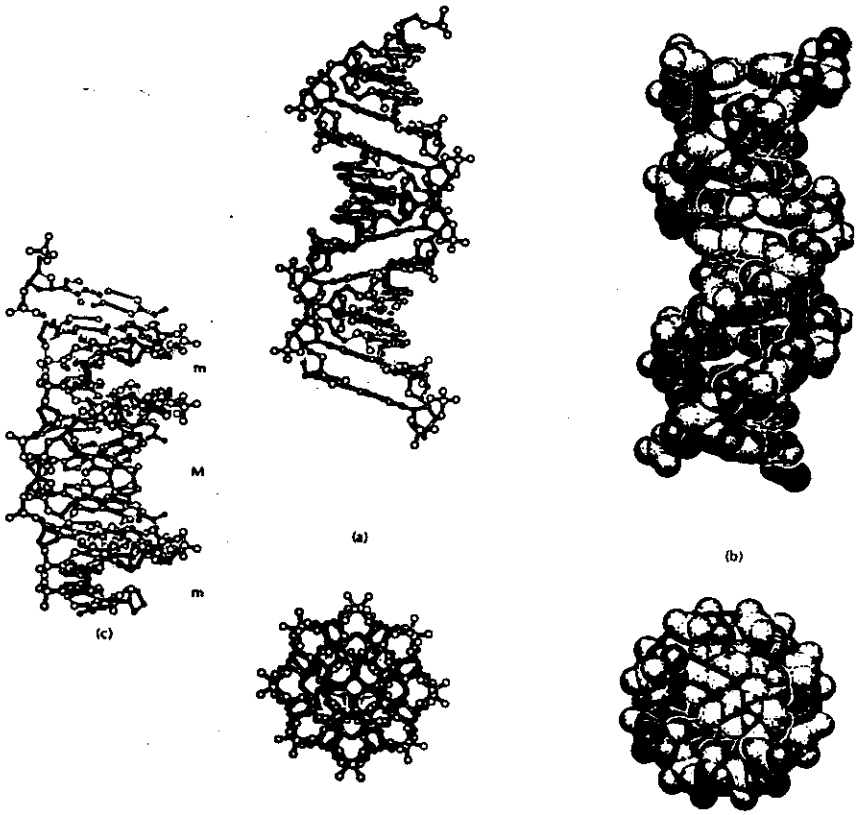

Figure 11- (a to c). Structure of D-DNA, drawn with atomic coordinates for poly(dA–dT) given in (845). For graphical details and scale, see the legend to Figure 11-2. (a and b) Side and top view of D-DNA as ball-and-stick and space filling plots; (c) the helix tilted 32° from the viewer to display geometry of minor (m) and major (M) grooves.

Fig. 11

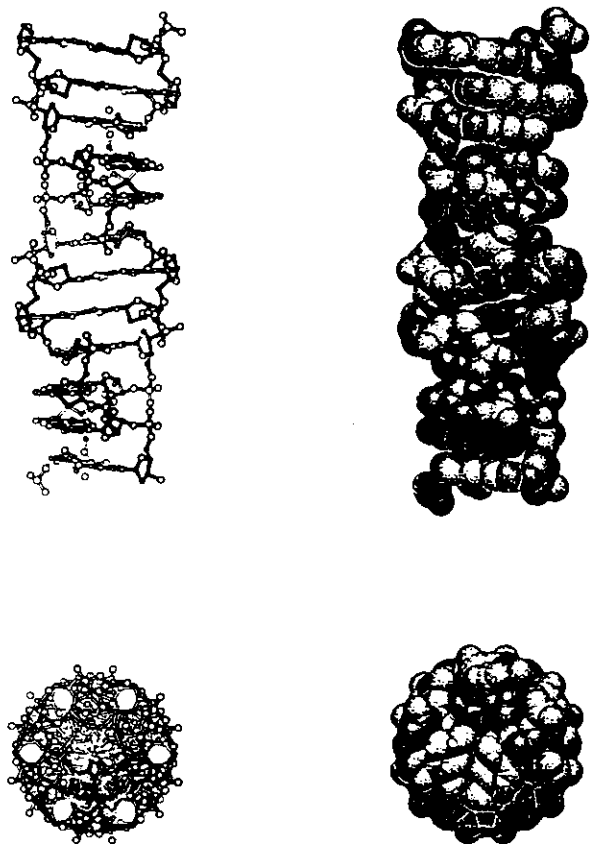

Figure 12- Molecular structure of the left-handed double-helical poly(DG–dC)·poly(dG–dC). Drawn with coordinates for Z_1-DNA derived on the basis of the hexanucleotide d(CGCGCG) in side and top view. For graphical details and scale, see legend to Figure 11-2.

Fig. 12

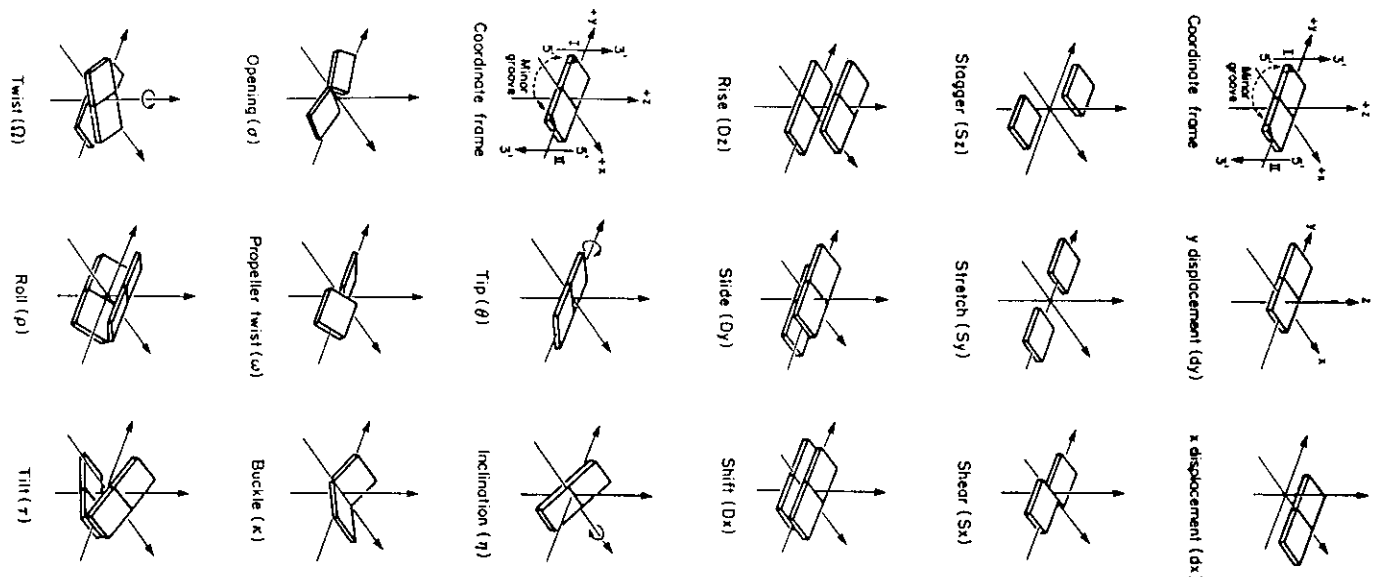

Fig. 13

HELICAL PARAMETERS FOR DIFFERENT DOUBLE-HELICAL POLYNUCLEOTIDES OBTAINED BY X-RAY FIBER DIFFRACTION METHODS

STRUCTURE	PITCH (Å°)	AXIAL RISE h (Å)	TWIST ANGLE t (°)	GROOVE WIDTH MINOR (Å)	GROOVE WIDTH MAJOR	GROOVE DEPTH MINOR (Å)	GROOVE DEPTH MAJOR
A	28.2	2.56	32.7	11.0	2.7	2.8	13.5
B	33.8	3.38	36.0	5.7	11.7	7.5	8.5
C	31.0	3.32	38.6	4.8	10.5	7.9	7.5
D	24.3	3.04	45.0	1.3	8.9	6.7	5.8
Z	45.0	3.70	-30.0	8.8	2.0	3.7	13.8

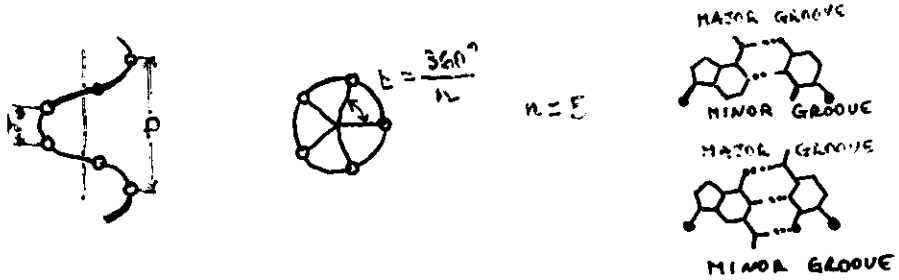

Fig. 14

HELIX AXIS DISLOCATION IN DIFFERENT CONFORMATION

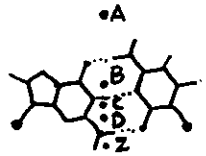

BASE STACKING (AT) IN DOUBLE HELICES AT DIFFERENT CONFORMATIONS

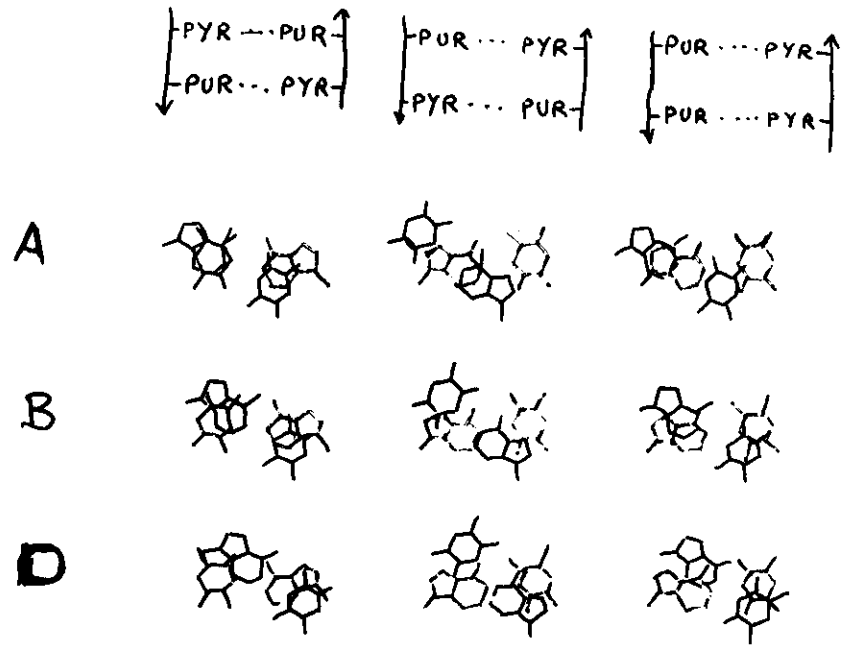

Fig. 15.1

Table 6-9. Prediction of DNA Double Helix Stability from Base Sequence [From (555)]

(A) Stability Matrix for Nearest-Neighbor Stacking in Base-Paired Dinucleotides in B-DNA Geometry*:

5' \ 3'	A	T	G	C
T	36.73	54.50	54.71	86.44
A	54.50	57.02	58.42	97.73
C	54.71	58.42	72.55	85.97
G	86.44	97.73	85.97	136.12

* Numbers give T_m values in °C at 19.5 mM Na^+.

(B) T_m Values Predicted with This Matrix for a Collection of Synthetic DNA Polymers with Defined Sequence:

Polynucleotide	T_m(°C) Experimental[a]	Calculated[b]	Difference[c]
Poly(dA-dT)·poly(dA-dT)	45.0	46.9	−1.9
Poly(dA-dA-dT)·poly(dA-dT-dT)	49.2	49.4	−0.2
Poly(dA)·poly(dT)	53.0	54.5	−1.5
Poly(dG-dA-dA)·poly(dT-dT-dC)	64.5	66.5	−2.0
Poly(dG-dT-dA)·poly(dT-dA-dC)	66.8	64.3	2.5
Poly(dA-dA-dC)·poly(dG-dT-dT)	70.2	69.0	1.2
Poly(dG-dA)·poly(dT-dC)	71.3	72.4	−1.1
Poly(dG-dA-dT)·poly(dA-dT-dC)	72.0	66.1	5.9
Poly(dG-dG-dA)·poly(dT-dC-dC)	76.3	76.9	−0.6
Poly(dG-dT)·poly(dA-dC)	77.4	76.2	1.2
Poly(dG)·poly(dC)	87.8	86.0	1.8
Poly(dG-dC)·poly(dG-dC)	99.2	104.3	−5.1

[a] Experimental melting temperatures at various ionic strengths are interpolated to 19.5 mM Na^+.
[b] Calculated from values in Table 6-9(A) and nearest-neighbor frequencies in each polymer.
[c] T_m (experimental) − T_m (calculated).

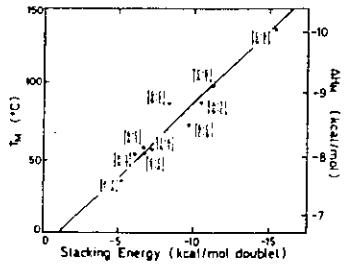

Figure 6-20. Correlation diagram between experimental melting temperatures T_m (Table 6-9) and theoretically evaluated stacking energies (Table 6-8) of base-paired dinucleotides in B-DNA geometry. Note that two different approaches to the same problem yield a satisfactory correlation with a correlation coefficient of 0.97. Stacking energies for dinucleotide duplexes entered in this plot differ slightly from data in Table 6-8 because different results given in Ref. (536) were used. From (555).

FIG. 15.2

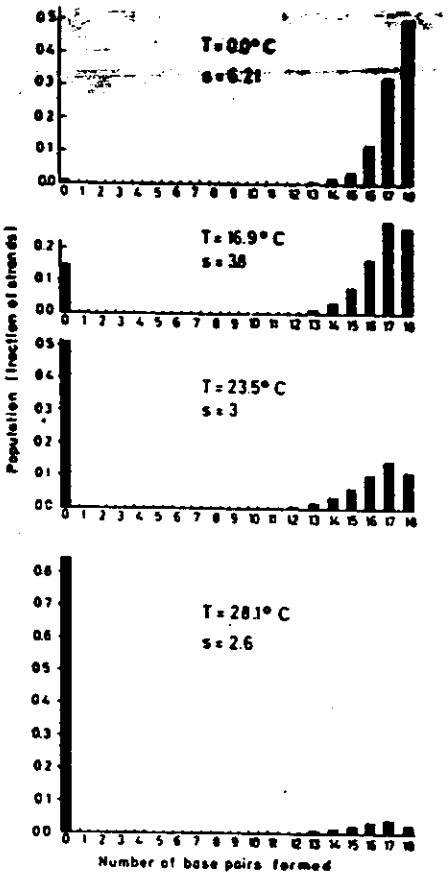

Figure 6-15. Population analysis for the system $A(pA)_{17} \cdot U(pU)_{17}$ at different temperatures. Product of [(nucleation parameter β) × (concentration ç)] used in this analysis is $\beta \cdot c = 10^{-7}$. Note that base-pairs at ends of the helix open and close easily, giving rise to a distribution of helices with 13 to 18 base-pairs but helices with 1 to 12 base-pairs are practically not observed; they either dissociate or form helices with 13 to 18 base-pairs. From (548).

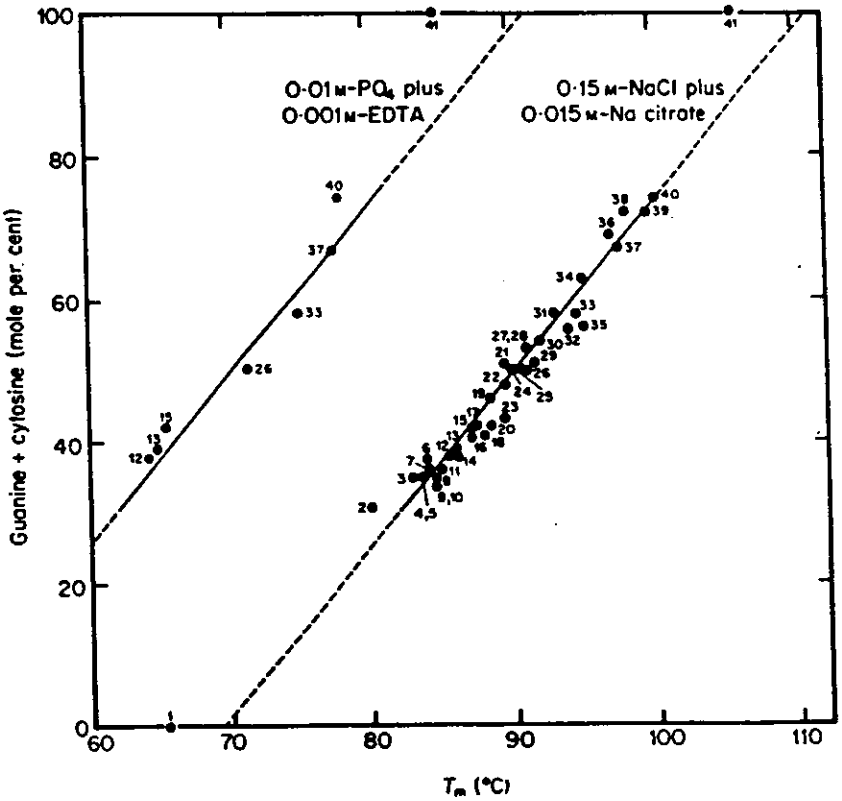

Figure 6-17. Dependence of melting temperature T_m on guanine + cytosine (G + C) content of various samples of DNA obtained from different sources. DNA was dissolved in 0.15 *M* NaCl + 0.015 *M* Na-citrate, pH 7.0. Points 1 and 41, for poly(dA-dT) and poly(dG-dC), fall off the least-squares line which is described

FIG 15.3

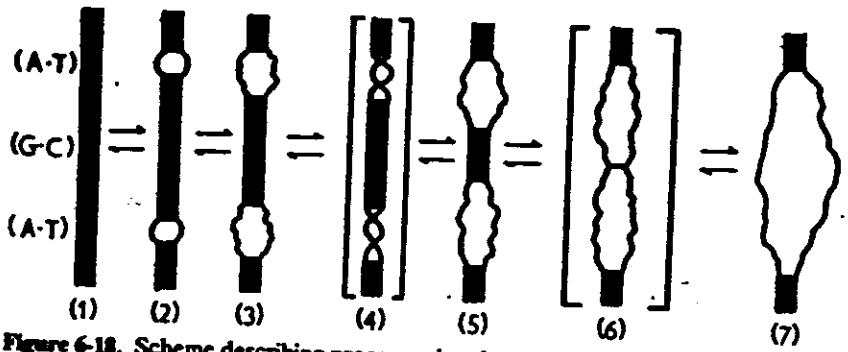

Figure 6-18. Scheme describing processes involved in DNA or RNA double-helix de- and renaturation. A–T-rich regions melt first, giving rise to states (2) and (3). In (4), additional base-pairs are opened and the twist is taken up in coil regions. From (550).

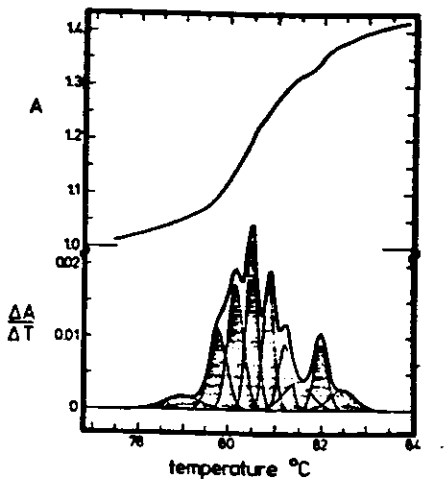

Figure 6-19. Melting profile of DNA (top) and its first derivative dA/dT (bottom). The latter curve is deconvoluted into nine individual peaks characterized by temperature, amplitude, and breadth. *A* indicates UV absorption at 260 nm; dA/dT or ΔA/ΔT are first derivatives with respect to temperature *T*. These curves are simulated; for some realistic data see Ref. (557).

FIG. 15.4

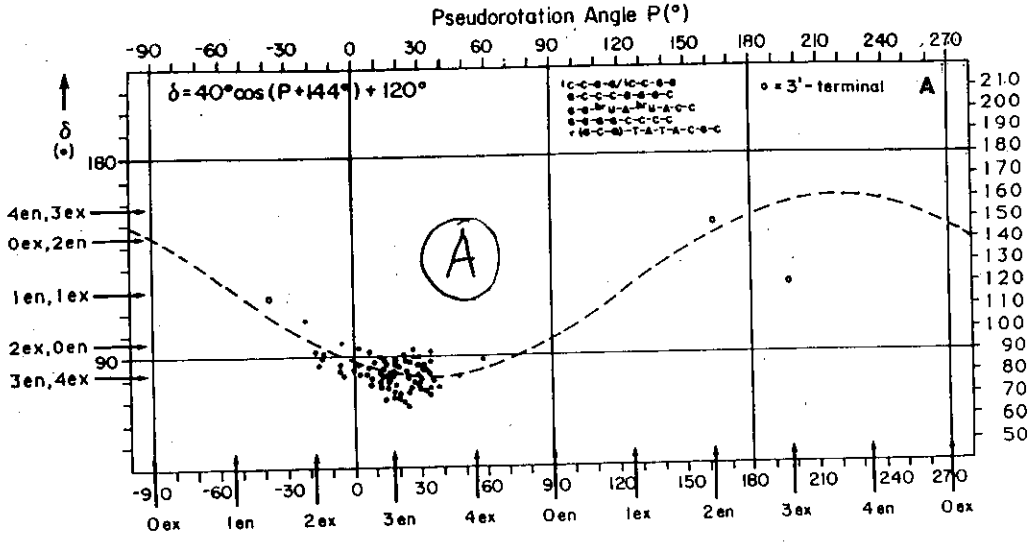

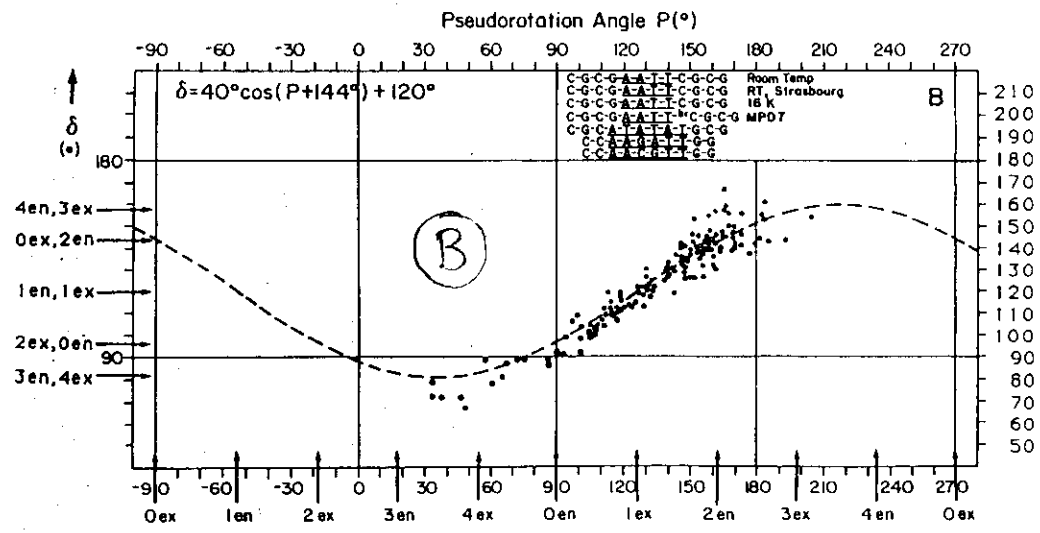

Fig. 16

CALLADINE RULE

IN ALTERNATING PUR-PYR OR PYR-PUR SEQUENCES BASE-PAIR PROPELLER TWISTS CAUSE CLASHES BETWEEN PURINES IN OPPOSITE STRANDS.

IN PUR-PYR G06 AND/OR AN6 IN THE MAJOR GROOVE

IN PYR-PUR GN3/N2 AND/OR AN3 IN THE MINOR GROOVE

THE LAST CLASH IS MUCH MORE SEVERE

THE CLASHES ARE REDUCED :

1. BY REDUCING PROPELLER TWIST
2. BY OPENING ROLL ANGLE
3. BY SHIFTING BASE-PAIR PARALLEL TO ITS LONG AXIS
4. BY DECREASING TWIST ANGLE TO 27°

STRATEGY (3) CHANGES SIMULTANEOUSLY BOTH χ AND δ TORSION ANGLES IN SUCH A WAY TO MANTAIN THE INTERPHOSPHATE DISTANCE AT A CONSTANT 6.7 Å, ACCORDING TO THE ANTICORRELATION PRINCIPLE

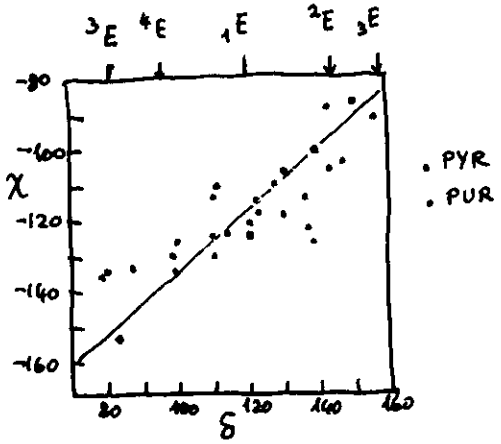

FIG. 16.1

ADJACENT BASE-PAIRS

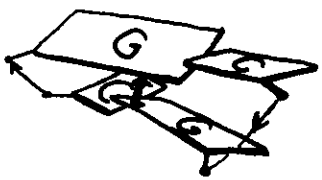

PYR - PUR

COMPRESSION OF MINOR GROOVE

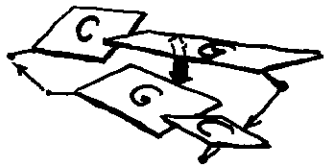

PUR-PYR

EXPANSION OF MINOR GROOVE

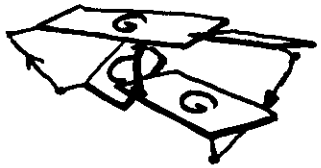

POSITIVE ROLL ANGLE

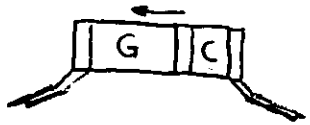

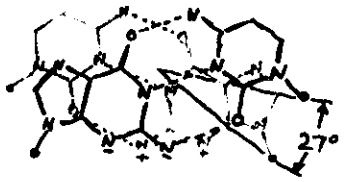

UNTWISTING FROM 36° TO 27°

Fig. 17

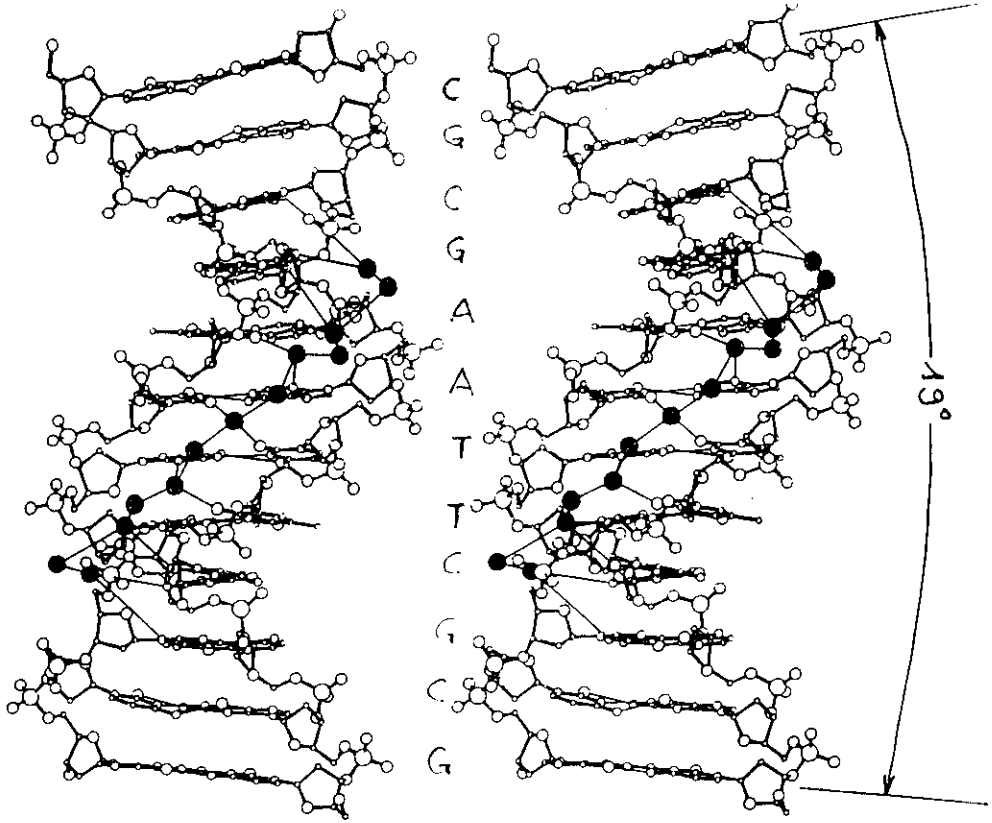

DREW DODECAMER SHOWING THE SPINE OF WATER MOLECULES (RED CROSSED SPHERES) DOWN THE NARROW MINOR GROOVE IN A REGION OF LARGE PROPELLER TWIST.

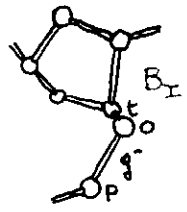

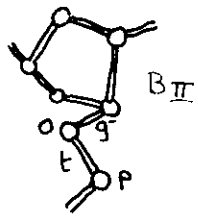

	ε	ζ
B I	t (180°)	g⁻ (240°)
B II	g⁻ (240°)	t (180°)

B II WIDENS THE MINOR GROOVE

Fig. 18.1

Table II.B Conformational (A), and Local Helical Parameters (B) for the B-DNA Dodecamer d(CGCGAATTCGCG). From (899,899a).

(A)

Residue	Angles, degrees χ	α	β	γ	δ	ε	ζ	Sugar pucker	Adjacent P-atom separation (Å)
C1	−105	—	—	174	157	−141	−144	C_2-*endo*	
G2	−111	−66	170	40	128	−186	−98	$C_{1'}$-*exo*	6.64
C3	−135	−63	172	59	98	−177	−88	$O_{4'}$-*exo*	6.47
G4	−93	−63	180	57	156	−155	−153	C_2-*endo*	6.83
A5	−126	−43	143	52	120	−180	−92	$C_{1'}$-*exo*	6.88
A6	−122	−73	180	66	121	−186	−89	$C_{1'}$-*exo*	6.90
T7	−127	−57	181	52	99	−186	−86	$O_{4'}$-*endo*	6.29
T8	−126	−59	173	64	109	−189	−89	$C_{1'}$-*exo*	6.87
C9	−120	−58	180	60	129	−157	−94	$C_{1'}$-*exo*	6.70
G10	−90	−67	169	47	143	−103	−210	C_2-*endo*	6.55
C11	−125	−74	139	56	136	−162	−90	C_2-*endo*	7.05
G12	−112	−82	176	57	111	—	—	$C_{1'}$-*exo*	
C13	−128	—	—	56	137	−159	−125	C_2-*endo*	
G14	−116	−51	164	49	122	−182	−93	$C_{1'}$-*exo*	6.62
C15	−134	−63	169	60	86	−185	−86	$O_{4'}$-*endo*	6.45
G16	−115	−69	171	73	136	−186	−98	C_2-*endo*	7.12
A17	−106	−57	190	54	147	−183	−97	C_2-*endo*	6.77
A18	−108	−57	186	48	130	−186	−101	C_2-*endo*	6.71
T19	−131	−58	174	60	109	−181	−88	$C_{1'}$-*exo*	6.70
T20	−120	−59	179	55	122	−181	−94	$C_{1'}$-*exo*	6.70
C21	−114	−59	185	45	110	−177	−86	$C_{1'}$-*exo*	6.17
G22	−88	−67	179	50	150	−100	−188	C_2-*endo*	6.60
C23	−125	−72	139	45	113	−174	−97	$C_{1'}$-*exo*	6.68
G24	−135	−65	171	47	79	—	—	C_3-*endo*	
Mean	−117	−63	171	54[a]	123	−169	−108		
±SD	14	8	14	8	21	25	34		
B DNA[b]	−119	−61	180	57	122	−187	−91		
B_FDNA[c]	−102	−41	136	38	139	−133	−157		
A_FDNA[c]	−154	−90	−149	47	83	−175	−45		

Base-pairs	Propeller twist, $°\theta_p$	Helix twist angle, °t[d]	Base-pairs per turn (n)	Rise per base pair, Å (h)
C1/G24	13.2 ± 2.0	38.3 ± 1.1	9.40 ± 0.27	3.36 ± 0.01
G2/C23	11.7 ± 2.1	39.6 ± 6.1	9.09 ± 1.40	3.38 ± 0.08
C3/G22	7.2 ± 2.1	33.5 ± 2.1	10.75 ± 0.67	3.26 ± 0.05
G4/C21	13.2 ± 1.9	37.4 ± 1.7	9.63 ± 0.44	3.30 ± 0.10
A5/T20	17.1 ± 2.1	37.5 ± 0.9	9.60 ± 0.23	3.27 ± 0.02
A6/T19	17.8 ± 2.1	32.2 ± 2.1	11.18 ± 0.73	3.31 ± 0.03
T7/A18	17.1 ± 1.9	36.0 ± 2.8	10.00 ± 0.78	3.29 ± 0.01
T8/A17	17.1 ± 2.0	41.4 ± 2.1	8.70 ± 0.42	3.14 ± 0.02
C9/G16	18.6 ± 1.9	32.3 ± 1.3	11.11 ± 0.45	3.56 ± 0.07
G10/C15	4.9 ± 1.9	44.7 ± 5.4	8.05 ± 0.97	3.21 ± 0.18
C11/G14	17.2 ± 1.9	37.0 ± 1.9	9.73 ± 0.50	3.54 ± 0.19
G12/C13	6.2 ± 2.3			
Mean	13.4 ± 4.9	37.3 ± 3.8	9.75 ± 0.98	3.33 ± 0.13
A DNA		32.7	11.0	2.56
B DNA		36.0	10.0	3.38
C DNA		38.6	9.33	3.31
D DNA		45.0	8.0	3.03

[a] C1 value omitted because it represents end effect.
[b] From the energy-refined B-DNA (836).
[c] From X-ray fiber diffraction data (304).
[d] Helical parameters obtained by using vectors between atoms $C_{1'}$ and attached N of one base and the equivalent atoms of the next nucleotide along the chain. Helical parameters are defined in Chapter 2.

FIG. 18.9

A		B (C, D)
$C_{3'}$-ENDO	SUGAR PUCKERING	$C_{2'}$-ENDO
5.9 Å	INTRAS. PHOSPHATE DISTANCE	7.0 Å
4.4 – 4.9 Å IN MAJOR GROOVE	DISLOCATION OF BASE-PAIRS FROM HELIX AXIS (D)	−0.2 ÷ −1.8 Å IN MINOR GROOVE
30 – 32.7°	ROTATION PER NUCLEOTIDE (t)	36-45°
2.56–3.29 Å	AXIAL RISE PER NUCLEOTIDE (h)	3.03 – 3.37 Å
+ 10 – 20°	BASE-PAIR TILT	−5.9° ÷ −16.4°
UNIFORM IN SHAPE	APPEARANCE	MORE ALTERED

OPEN CYLINDER INSIDE ($d \sim 3.5$ Å)

DEEP AND NARROW MAJOR GR.

SHALLOW AND WIDE MINOR GR.

STACK IS INTERSTR. AND INTRASTR. STACK IS ONLY INTRASTR.

SIZE AND DEPTH OF THE GROOVES CAN EXPLAIN SPECIFIC INTERACTIONS (METAL IONS, WATER, DIFFERENT MOIETIES)

ELECTROSTATIC POTENTIAL DUE TO CHARGE DISLOCATION INTO BASE PLANES CAN BE DEPENDENT ON BASE SEQUENCE AND ON GROOVE TYPE.

FIG. 18.3

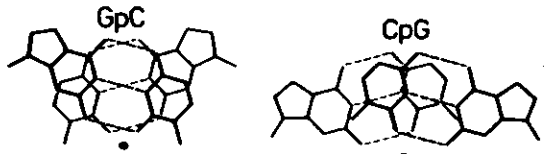

Figure 12-5. Stacking of adjacent bases in left-handed poly(dG–dC) poly (dG–dC) for sequences d(GpC), left, and d(CpG), right. Note that in d(GpC), intrastrand stacking between guanine and cytosine occurs and base-pairs are related by screw rotation. In contrast, in d(CpG) only interstrand stacking between cytosines is indicated and guanines interact with O_4 of adjacent deoxycytidine. Dots in minor groove represent location of helix axis. Drawn with Z_1-DNA coordinates given in (917).

Table 12-2. Concentrations of Cations or Ethanol at Midpoints of the B ⇌ Z Transition in Poly(dG-dC)·poly(dG-dC) and the Analog Containing Cytosine Methylated at C_5 (m^{5}C)

Ion	Poly(dG-dC)·poly(dG-dC)	Poly(dG-dm^{5}C)·poly(dG-dm^{5}C)
[a]Na^+	2500 m*M*	700 m*M*
Mg^{2+}	700 m*M*	0.6 m*M*
Ca^{2+}	100 m*M*	0.6 m*M*
Ba^{2+}	40 m*M*	0.6 m*M*
$Co(NH_3)_6^{3+}$	0.02 m*M*	0.005 m*M*
Spermidine^{3+}	Aggregates	0.05 m*M*
Spermine^{4+}	Aggregates	0.002 m*M*
Ethanol	60% (v/v)	20% (v/v)
[b]Mg^{2+} + 20% Ethanol	0.4 m*M*	
Mg^{2+} + 10% Ethanol	4 m*M*	

[a] From (927).
[b] From (924a).

FIG 19

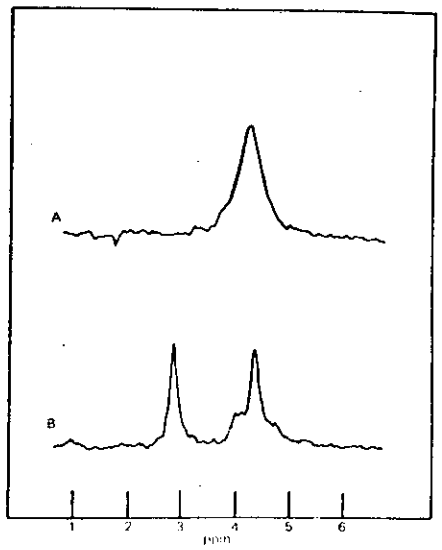

FIG. 5. The 14.7 MHz Fourier transform NMR spectra (1.6 ppm upfield from standard trimethylphosphate) for (dG-dC)$_3$ in 1 mM cacodylate/0.1 mM EDTA/1.0 m the presence of 0.7 M NaCl, pH 6.7, 27°C (spectrum A) and 4.6 M NaCl, pH 6.0, 27°C (spectrum B).

Table III. Structural Parameters for Z-DNAs

	Helix		
	Z_t	Z_α	Z_P
Bases per turn	12	12	12
Pitch height (Å)	44.6	44.6	43.5
Rotation per dinucleotide repeat (°)	−60	−60	−60
Rise per dinucleotide repeat (Å)	7.43	7.43	7.25
Base tilt (°)	−7	−7	−5
Radius (Å) of phosphate			
d(CpG)	6.3	6.1	
d(GpC)	7.3	8.0	

Torsion angle (°)

	Z_t		Z_α		Z_P		Z′		Z	
	pG	pC	pG	pC	pG	pC	pG	pC	pG	pC
α	47	−137	92	146	52	−110	75	177	70	−175
β	179	−139	−167	164	−153	−168	175	−166	−174	−168
γ	−165	56	157	66	178	54	−178	51	176	61
ϑ	99	138	94	147	76	147	122	141	97	143
ϵ	−104	−94	−179	−100	−72	−103	−150	−85	−142	−97
ζ	−69	80	55	74	102	−91	−17	71	−7	77
χ	68	−159	62	−148	89	−159	70	−160	65	−154

Note. Data for Z_t and Z_α were derived on the basis of the d(CpGpCpGpCpG) crystal structure; those for Z- and Z′-DNA are from the analogous tetramer (302,303,917,918), and data for Z_P are from a fiber diffraction study (304).

PURINES: $C_{3'}$-endo syn
PYRIMIDINES: $C_{2'}$-endo anti

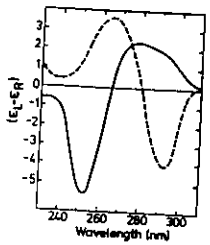

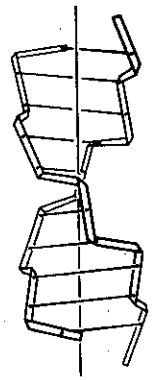

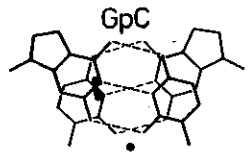

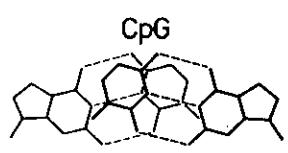

FIG. 20

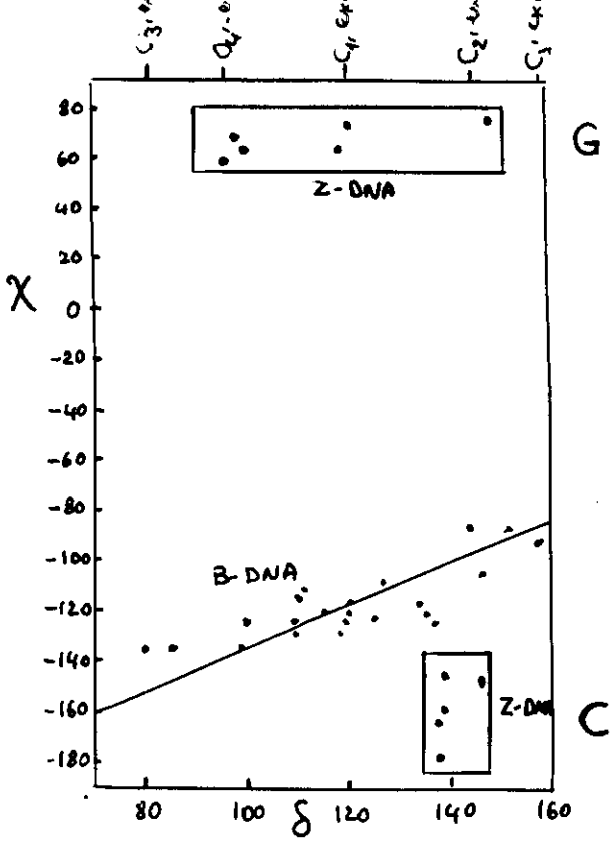

Fig. 21

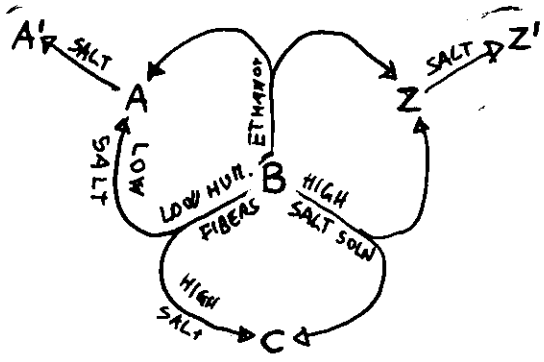

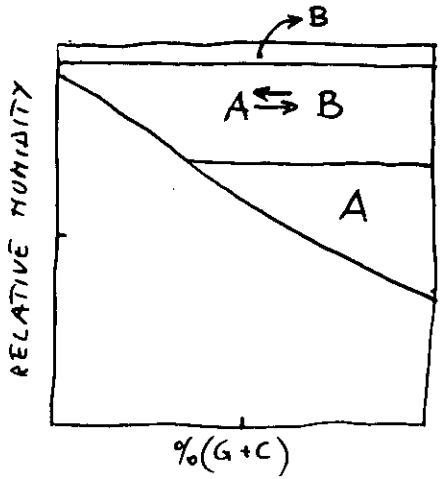

FIG. 21.1

DNA FLEXIBILITY

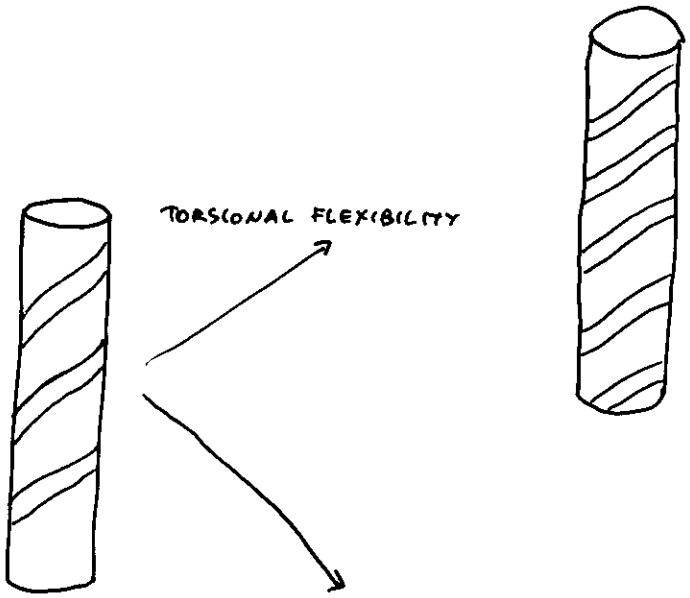

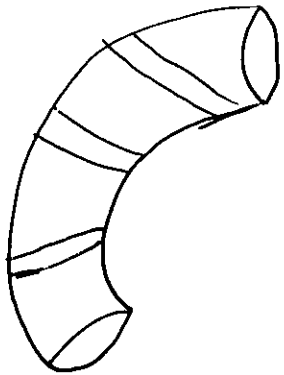

WINDING → LESS BASES PER TURN → NARROW MINOR GROOVE → LARGER MAJOR GROOVE (A-T RICH REGIONS)

UNWINDING → MORE BASES PER TURN → LARGER MINOR GROOVE → NARROWER MAJOR GROOVE (G-C RICH REGIONS)

FIG. 21.2

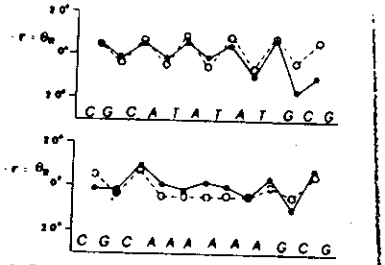

Fig. 2. Comparison of the roll angles obtained by conformational analysis, r (○) with those obtained by X-ray diffraction analysis, Θ_R (●) (the sign of r is inverted because of a different convention adopted) [30].

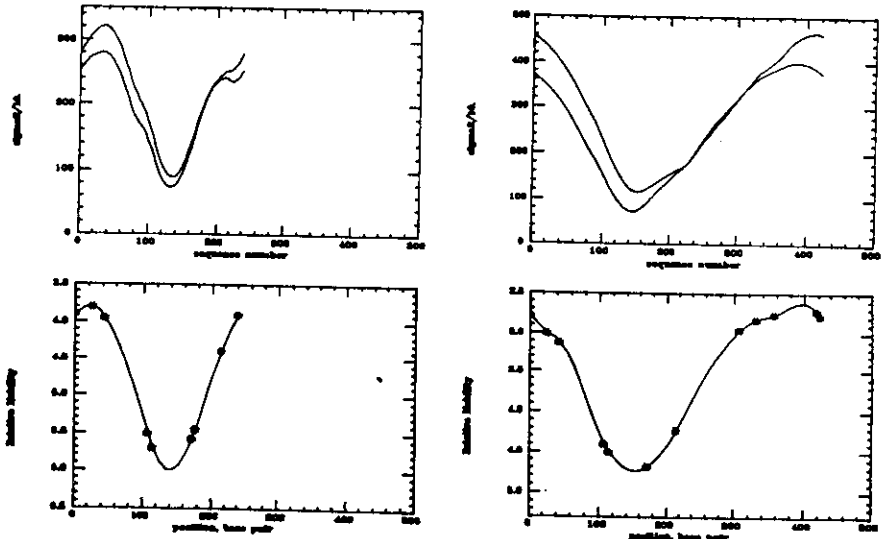

FIGURE 3: Comparisons between the theoretical gel electrophoresis permutation diagrams of two fragments of K-DNA (1–241 and 1–423) as calculated by use of our old and the refined matrices for roll, tilt, and twist. The diagrams below are the experimental gel electrophoresis as reprinted by Wu and Crothers (1984).

FIG. 22

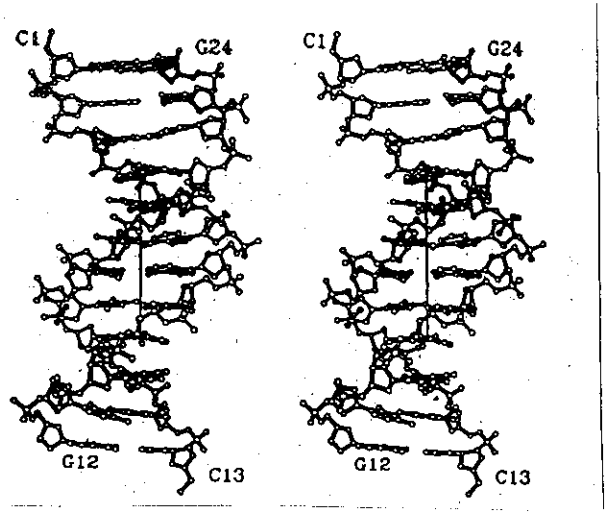

ρ	A	T	G	C
T	8.0	-5.4	6.7	2.0
A	-5.4	-7.3	1.0	-2.4
C	6.7	1.0	4.6	1.3
G	2.0	-2.4	1.3	-3.7

τ	A	T	G	C
T	0.0	0.5	-0.4	1.7
A	-0.5	0.0	-1.6	-2.7
C	0.4	1.6	0.0	0.6
G	-1.7	2.7	-0.6	0.0

Ω	A	T	G	C
T	34.6	35.9	34.5	35.8
A	35.9	35.0	35.6	34.6
C	34.5	35.6	33.7	33.0
G	35.8	34.6	33.0	33.3

Fig.23

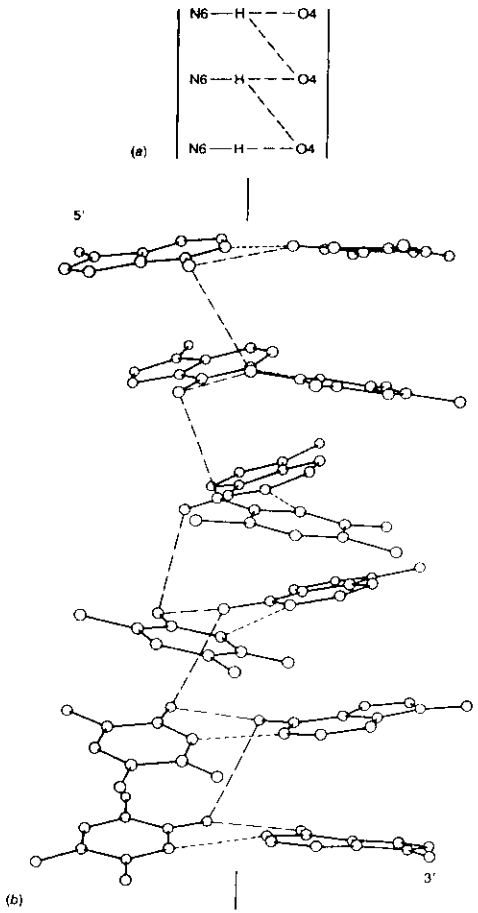

Figure 1.7 The structure of an oligo dA:dT tract. Bifurcated hydrogen bonding between N6 of adenine and O4 of thymine (a) is made possible by the propeller twisting of the A-T base pairs (b).

FIG 23.1

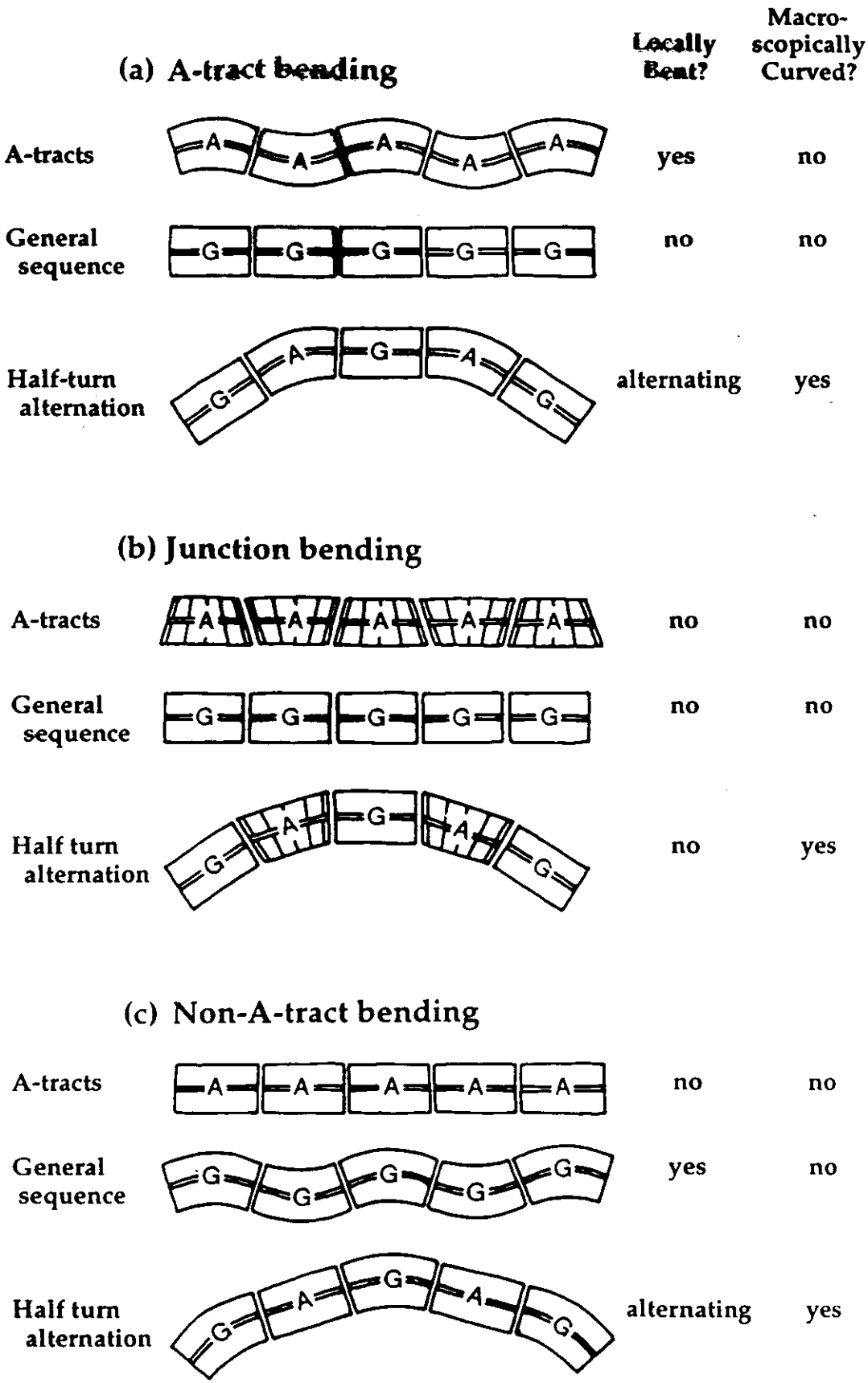

Fig. 10.

FIG. 23.2

Table 3

Analysis of gel mobility in T_nA_n tracts

Helix	Bend spacing	Angle θ (°)	2 cos(θ/2)	(R_L-1)	A-tract deduction
G-C-A-A-A-A-T-T-T-T *	1 bend	n/a	1·00†	1·56	
C-G-A-A-A-A-T-T-T-T *	1 bend	n/a	1·00†	1·30	
T-T-T-T-T-A-A-A-A-A *	1 bend	n/a	1·00†	0·55	Not roll-wedge
C-G-T-T-T-T-A-A-A-A * *	5·0 bp	180	0·00	0·20	Not tilt-wedge
G-C-T-T-T-T-A-A-A-A * *	5·0 bp	180	0·00	0·12	
T-G-G-G-C-A-A-A-A-A *	1 bend	n/a	1·00†	1·08	
C-C-G-C-T-A-A-A-A-A * *	3·0 bp	108	1·18	0·93	
C-C-C-T-T-A-A-A-A-A * *	3·5 bp	126	0·91	0·80	
C-C-T-T-T-A-A-A-A-A * *	4·0 bp	144	0·61	0·58	
C-T-T-T-T-A-A-A-A-A * *	4·5 bp	162	0·31	0·09	

Bends are placed at the T-A step and at the centers of non-A tracts, marked by an asterisk (*) below each base sequence. The angle (θ) between directions of 2 bends is approximated by 36° times the number of base-pairs separating the bends. The vector sum of 2 bends is given by 2 cos(θ/2). R_L, the gel retardation factor, is the ratio of apparent to true molecular weight of the oligonucleotide, as gauged by migration velocity through the gel. (R_L-1) is the gel anomaly, zero for linear oligomers and positive for bent molecules. (R_L-1) values for first 5 entries are from Hagerman (1986, 1988); those for last 5 entries from Haran & Crothers (1989). Experimental (R_L-1) values are closely matched by the vector sum of the 2 bends, 2 cos(θ/2).

n/a, not applicable.

† Only one bend per turn of helix.

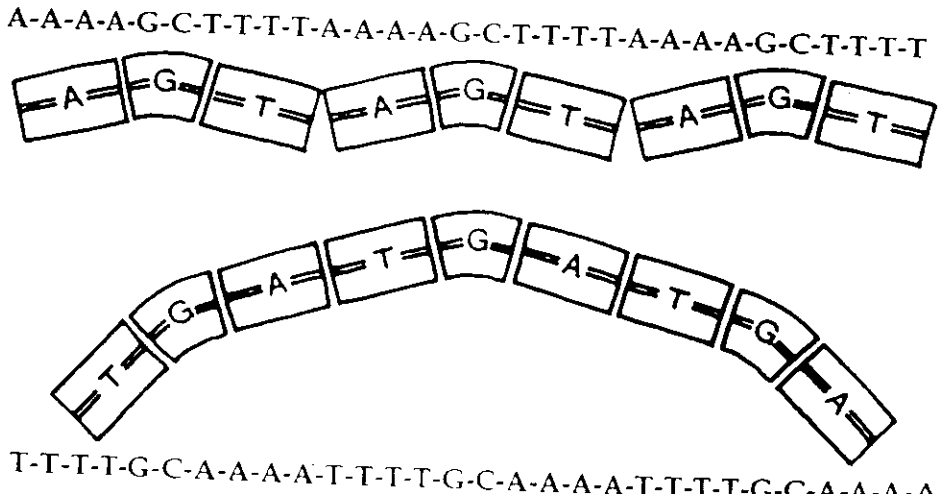

Figure 11. The influence of the order of A_4 and T_4 blocks on DNA bending. The sequence (C-G-T-T-T-T-A-A-A-A)$_n$ is macroscopically uncurved because the natural 6° roll bend at a G-C step is counterbalanced a half-turn away by the natural 6° roll bend of a T-A step. Both bends involve roll compression of the major groove. A-tract segments T-T-T-T and A-A-A-A are straight and unbent. The sequence (C-G-A-A-A-A-T-T-T-T)$_n$ is curved because the A-T step, like the other A-tract steps, is unbent and offers no compensation for the bent G-C steps phased every turn of helix.

FIG. 23.3

LOCAL DNA CONFORMATION AND PROTEIN BINDING

DNase I

- DNase I CUTS POLY dA · POLY dT AND POLY dG · POLY dC AT LOW RATE DUE TO THEIR CONFORMATIONAL RIGIDITY
- DNase I CLEAVES DNA WITH DIFFERENT EFFICIENCY ALONG A GIVEN SEQUENCE
- DNase I CLEAVES DNA IN THE MINOR GROOVE
- WHEN DNase I CUTS A CIRCULAR DNA WITH A VERY HIGH RADIUS OF CURVATURE IT DOES WHERE THE MINOR GROOVE IS OUTSIDE THE CIRCLE, NOT INSIDE
- WHEN A DNA IS WRAPPED AROUND A PROTEIN DNase I CUTS AN EXPOSED MINOR GROOVE BETTER THAN IN FREE DNA

DNase RECOGNIZES DNA THROUGH A WIDENED (FROM 11 TO 15 Å) MINOR GROOVE, WHICH OFTEN MEANS A BENT DNA

TOPOISOMERASE I.

- IN EUKARYOTES TOPO I RELAXES BOTH POSITIVE AND NEGATIVE SUPERCOILS
- IN PROKARYOTES TOPO I RELAXES ONLY NEGATIVE SUPERCOILS
- EUKARYOTIC TOPO I ACTS ALSO ON INTRINSICALLY BENT BUT RELAXED DNA

EUKARIOTIC TOPO I RECOGNIZES DNA BENT BY THE TORSIONAL STRESS (E.G. RECOGNIZES WRITHE)

PROKARIOTIC TOPO I RECOGNIZES BASE STEPS UNWOUND BY TORSIONAL NEGATIVE STRESS

FIG. 23.4

NUCLEOSOME POSITIONING OR PHASING

- THE NUCLEOSOMES CAN BE ASSEMBLED WITH AN IMMENSE VARIETY OF DNA SEQUENCES
- HOWEVER THE HISTONE OCTAMER CAN POSITION ITSELF WITH RESPECT TO A DEFINED DNA SEQUENCE
- THE FACTOR WHICH GUIDES THE MECHANISM IS BENDABILITY

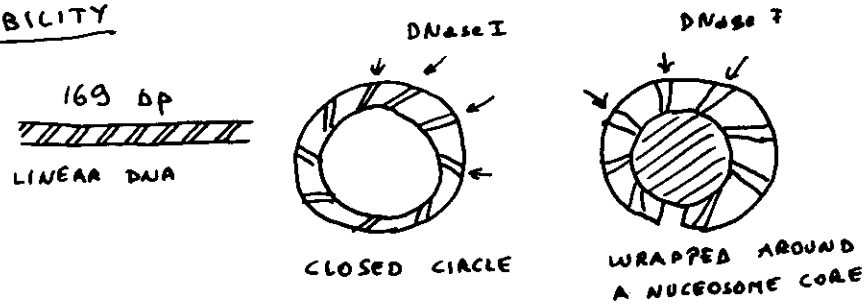

BENDABILITY IS THE MAJOR DETERMINANT OF NUCLEOSOME POSITIONING.

WHEN DNA WRAPES A HISTONE OCTAMER THE INTERNAL CIRCUMFERENCE IS 207 Å WHEREAS THE EXTERNAL ONE IS 333 Å. THIS IMPLIES THAT MINOR AND MAJOR GROOVE ON THE EXTERIOR SURFACE BE WIDENED WHEREAS THE INTERNAL ONES BE COMPRESSED. AS THE LAST MECHANISM IS EASIER FOR AT RICH SEQUENCES ONE WOULD EXPECT THAT THESE SEQUENCES ARE STATISTICALLY DISTRIBUTE EVERY 10 bp. THIS HAS BEEN FOUND EXPERIMENTALLY.

FIG. 23.5

A SERIES (~200) OF DNA FRAGMENTS OF 145 bp OBTAINED FROM DIGESTION OF CHROMATIN WERE PROBED WITH MOLECULES WHICH BIND PREFERENTIALLY TO AT RICH OR TO GC RICH SEQUENCES, AND THEN TREATED WITH DNase I. THE DRUG MOLECULES PROTECTED DNA FROM DNase I ACTION

THE GEL ELECTROPHORESIS PROFILES SHOWED THAT THE PROTECTION HAD A TEN BASE PERIODICITY WITH OPPOSITE PHASE

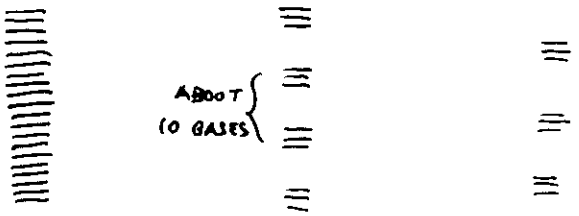

CLONING AND SEQUENCING THE SAME DNA FRAGMENTS GAVE THE FOLLOWING RESULTS

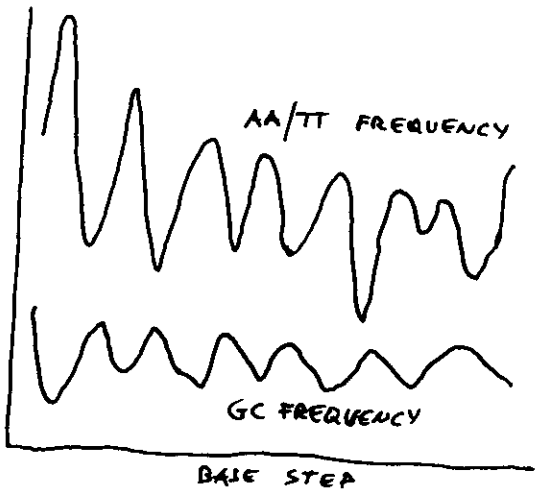

FIG. 23.6

EUKARYOTIC S1 HYPERSENSITIVE SITES

CHICKEN β GLOBIN GENE	GGGGAAGAGGAGGGG
RAT PREPROINSULIN II GENE	GGGGTCA GGGG
SV40 ENHANCER	GGGGAGCCTGGGG
DROSOPHILA HSP 26	AGAGAGAGAAAGAGAAGAGAGAGA
" " 22	TCTCTCCCACTCTCT
" " 70 pHTΔ5'	CTCTCTTTTCTTTTTGGGTCTCTC
" " 70 pHT1	CTCTCTGTACTATTGCTCTCTC
ADENOVIRUS MAJOR LATE PROM. Ad 2	GGGGGCTATAAAAGGGGG
" " " Ad 7	GGGGGTATAAAAGGGGG
" " " Ad 12	GGGGTATAAAAAGGG
HUMAN c-myc GENE	CCCTCCCCATAGCGCCCCTCCC
HUMAN α2-α1 GLOBIN INTERG. REGION	CCTCCTCCACCTCCTCC
CHICKEN α2(I) COLLAGEN PROMOTER	TCCCTCCCCTTCCTCCCTCCCT

MIRROR SEQUENCES
+ FANCIER BASES

PURINES
PYRIMIDINES

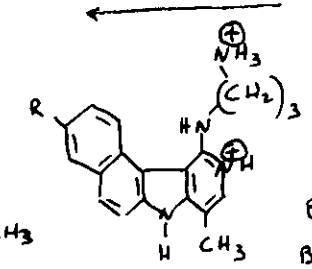

R = OCH3

BPI
BENZOPYRIDOINDOLE DERIVATIVES
INTERCALATE INTO TRIPLE HELICES
AND STABILIZE THEM

FIG. 23.7

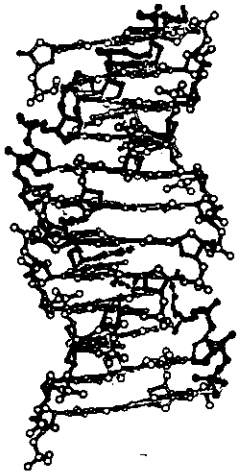

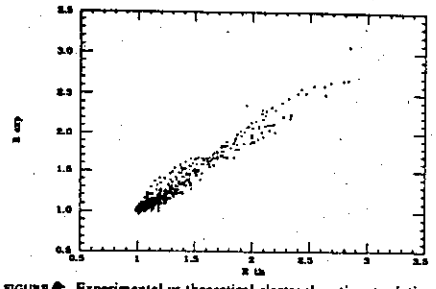

FIGURE 6: Experimental vs theoretical electrophoretic retardation factors for 450 synthetic multimeric oligonucleotides with 62 different sequences ranging between 50 and 200 bp. $Rth = 0.97 + (1.56 \times 10^{-4})\sigma^2$ (correlation coefficient = 0.98)

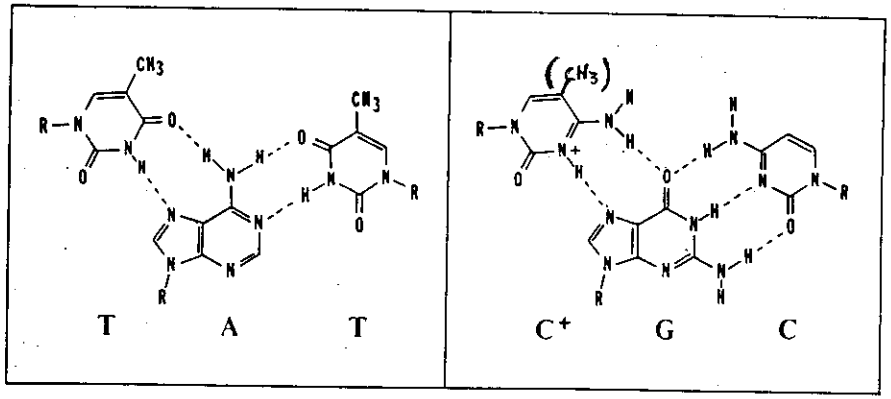

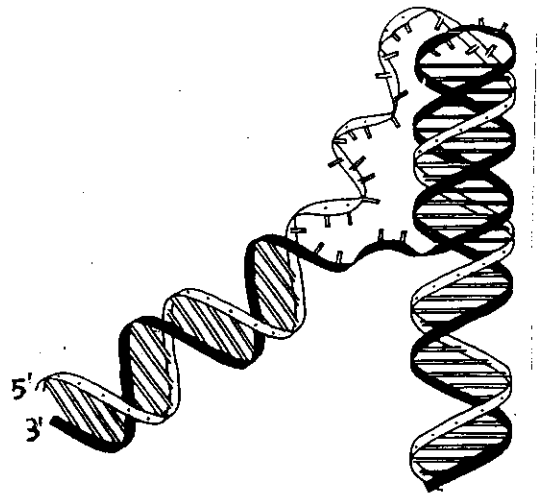

WHEN ANTI AND HOOGSTEEN THE THIND STRAND HAS A PARALLEL ORIENTATION WITH RESPECT TO THE HOMOPURINE STRAND - SYN AND/OR REVERSE HOOGSTEEN REVERSE ORIENTATION.

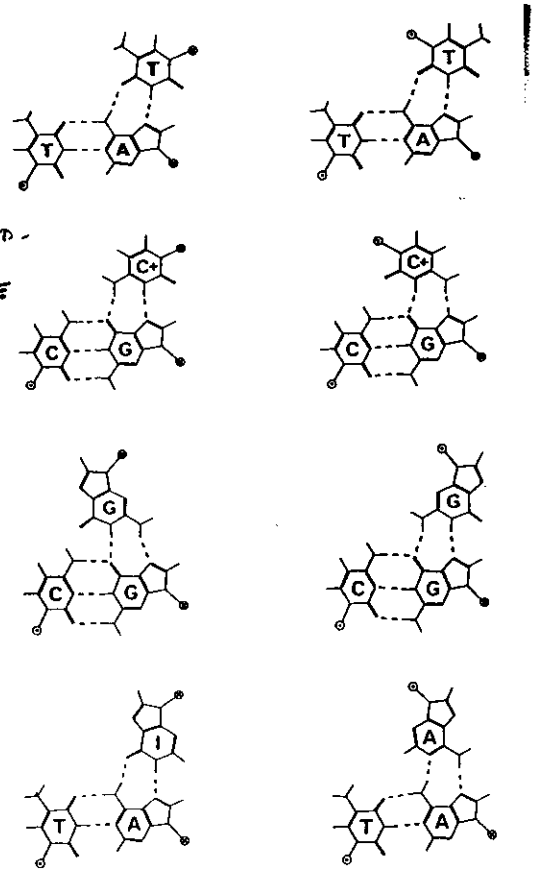

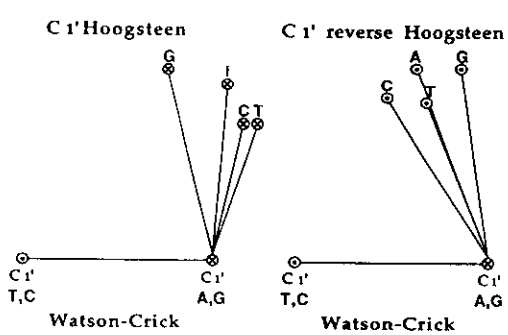

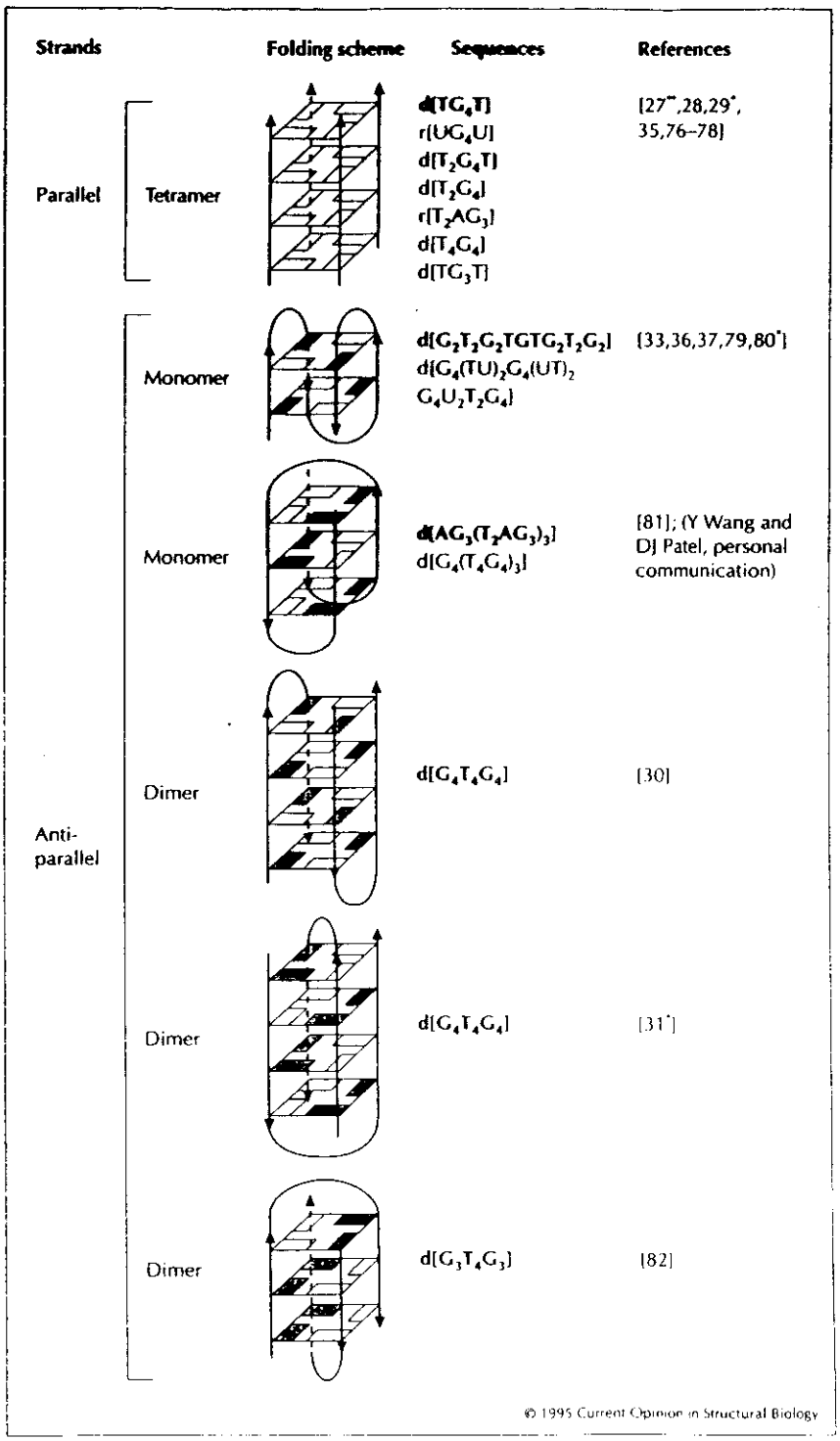

Fig. 1. Schematic representation of the G-quadruplex structures that can be adopted by telomeric G-strand sequences ([27••, 28,29•,30,31,33,35–37,76–79,80•,81,82] as shown). Sequences have been grouped into families of structures; the structure shown is that of the sequence in bold. The bases are represented by rectangles and both the number and the orientation of G-strands are indicated. *Syn* guanines are shown shaded; *anti* guanines are shown as open rectangles.

FIG. 26

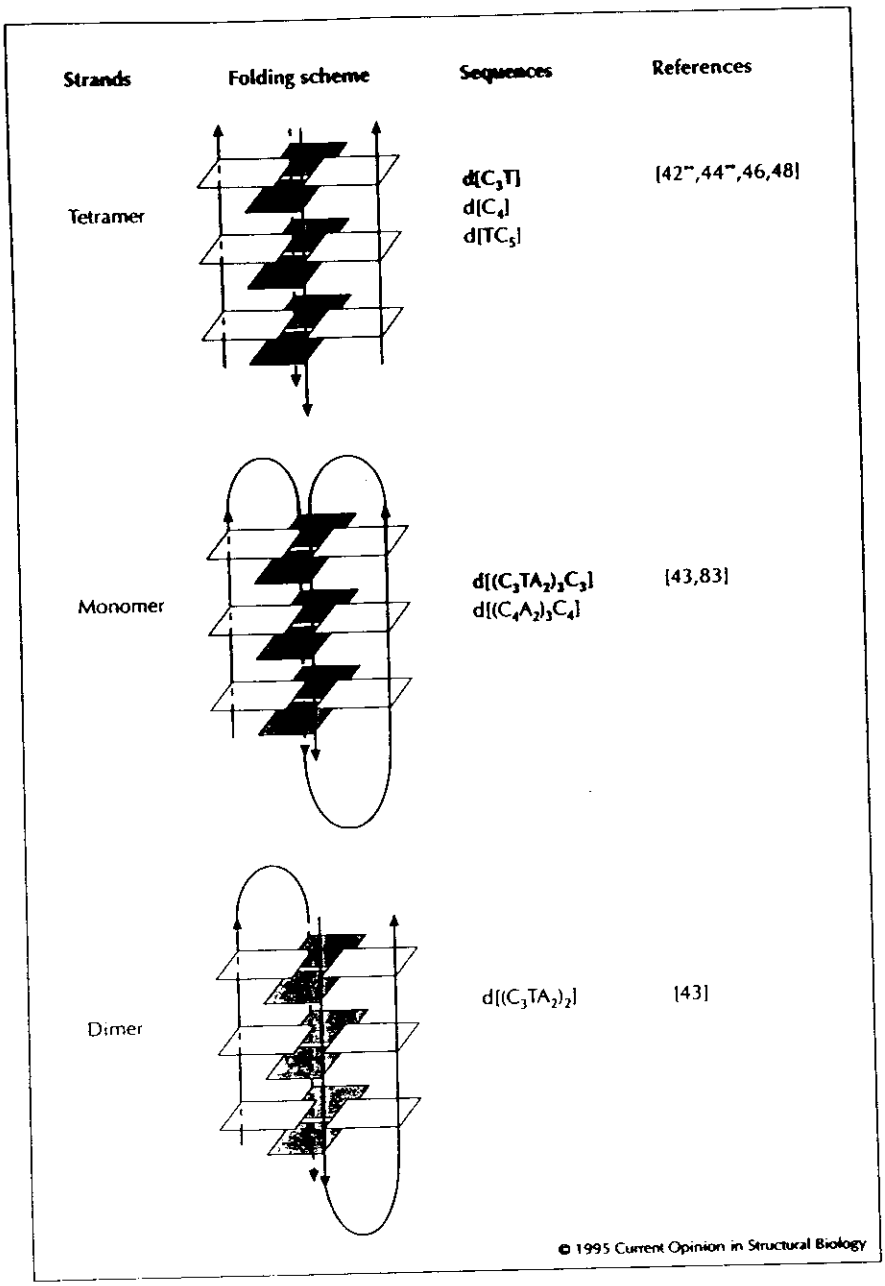

Fig. 5. Schematic representation of the i-tetraplex structures that can be adopted by telomeric C-strand sequences ([42••, 43,44••,46,48,83] as shown). The bases are represented by rectangles and alternate C–C$^+$ base pairs are shaded for clarity. Note that the dimeric and intramolecularly folded i-tetraplexes are models based on the results of biochemical and NMR studies, and are not fully determined three-dimensional structures.

FIG. 27

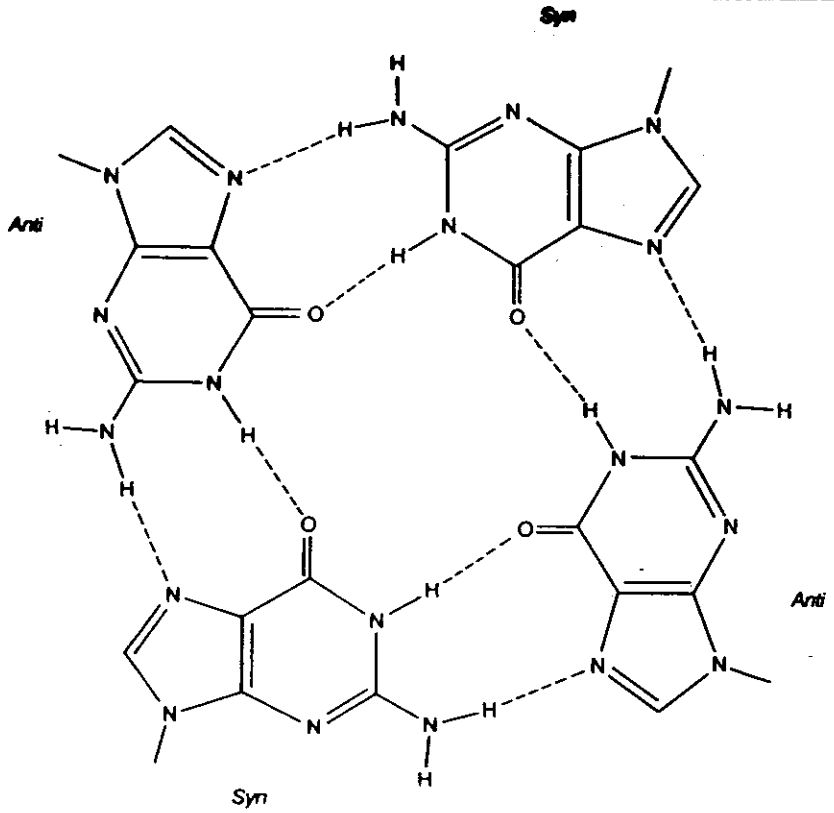

Figure 1.18 (b) The structure of a guanine quadruplex.

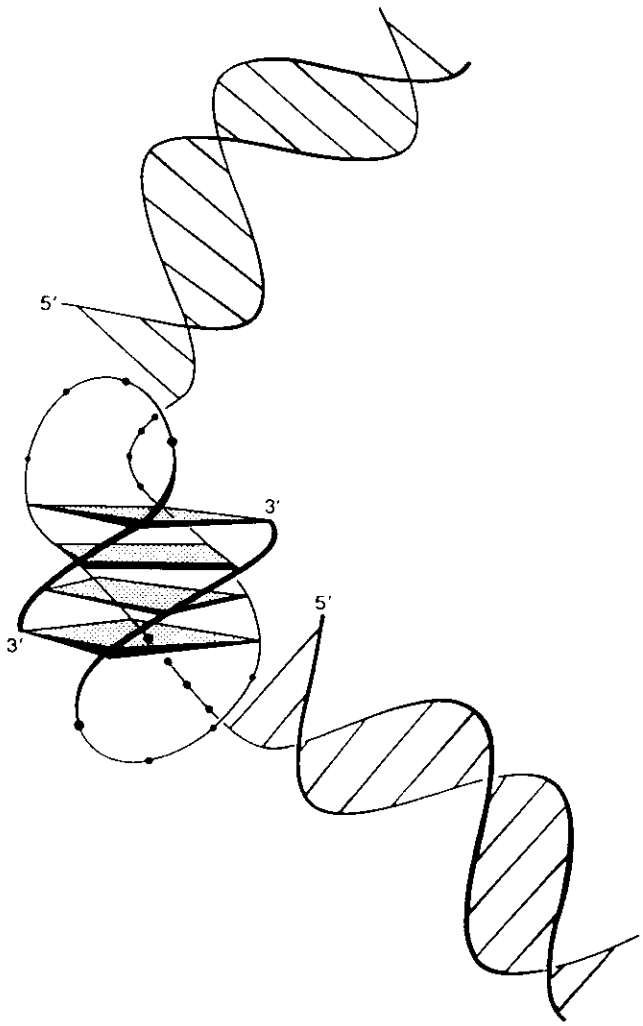

FIG. 28